Bismuth-based drugs sensitize *Pseudomonas aeruginosa* to multiple antibiotics by disrupting iron homeostasis

Yushan Xia [1,2,3], Xueying Wei [1], Peng Gao [4], Chenyuan Wang [1],
Anne de Jong [2], Jonathan Hon Kwan Chen [4,5],
María José Rodríguez-Sánchez[6], Alba Rodríguez-Nogales[7],
Patricia Diez-Echave[7], Julio Gálvez[7,8], Federico García [9,10], Weihui Wu[3],
Richard Yi-Tsun Kao[4], Hongyan Li [1], Rubén Cebrián [2,9] ✉,
Oscar P. Kuipers [2] ✉ & Hongzhe Sun [1] ✉

Pseudomonas aeruginosa infections are difficult to treat due to rapid development of antibiotic drug resistance. The synergistic combination of already-in-use drugs is an alternative to developing new antibiotics to combat antibiotic-resistant bacteria. Here we demonstrate that bismuth-based drugs (bismuth subsalicylate, colloidal bismuth subcitrate) in combination with different classes of antibiotics (tetracyclines, macrolides, quinolones, rifamycins and so on) can eliminate multidrug-resistant *P. aeruginosa* and do not induce development of antibiotic resistance. Bismuth disrupts iron homeostasis by binding to *P. aeruginosa* siderophores. Inside cells, bismuth inhibits the electron transport chain, dissipates the proton motive force and impairs efflux pump activity by disrupting iron–sulfur cluster-containing enzymes, including respiration complexes. As a result, bismuth facilitates antibiotic accumulation inside bacteria, enhancing their efficacy. The combination therapy shows potent antibacterial efficacy and low toxicity in an ex vivo bacteraemia model and increases the survival rate of mice in in vivo mouse lung-infection models. Our findings highlight the potential of bismuth-based drugs to be repurposed to combat *P. aeruginosa* infections in combination with clinically used antibiotics.

Rising antimicrobial resistance (AMR) in community-acquired and intrinsic drug-resistant pathogens poses a major challenge to global healthcare systems[1–3]. This is particularly evident in drug-resistant Gram-negative bacterial infections. *Pseudomonas aeruginosa*, a ubiquitous opportunistic pathogen, is notably resistant to antibiotics[4], causing severe infections in vulnerable patients such as those who are immunocompromised, in intensive care unit, with burn wounds or with cystic fibrosis[5]. Resistance in *P. aeruginosa* is primarily due to its restricted outer membrane permeability, multiple drug efflux pumps and antibiotic-inactivating enzymes[6]. The clinical challenge is worsened by chronic biofilm infections and the bacterium's ability to adapt its metabolism to the local microenvironment, leading to infection relapses and recurrent antibiotics resistance[7].

Despite notable efforts being made, few new antibiotics for Gram-negative bacterial infections have been approved in recent decades[8–10]. This creates an urgent need for novel antimicrobials or

alternative strategies. Repurposing existing drugs to enhance the efficacy of current antibiotics is a promising and economic approach to address the AMR crisis[11,12]. Combinatory therapy with antibiotics and adjuvants is an effective strategy to enhance antibiotic efficacy, prolong the utility of current antibiotics and delay the emergence of drug-resistant strains[13]. These synergistic therapies can also reduce antibiotic toxicity, duration of treatment and dosage requirements[14].

Historically, bismuth compounds have treated ailments such as syphilis, malaria and wound infections and are currently used for peptic ulcers linked to *Helicobacter pylori*[15–17]. It is worth noting that combining bismuth with antibiotics is an effective clinical therapy for eradicating *H. pylori*, including resistant strains[18], by inhibiting multiple proteins/enzymes, cell wall synthesis, adenosine triphosphate (ATP) synthesis and bacterial adhesion to the gastric mucosa[19]. However, the use of bismuth compounds for *H. pylori* treatment is mostly empirical. Recent studies show that bismuth drugs can be repurposed to treat metallo-β-lactamase-positive or tigecycline-resistant bacterial infections by inhibiting metallo-β-lactamases and tetracycline inactivation enzyme[20,21]. This suggests that bismuth–antibiotic combinations could address resistance in bacteria beyond *H. pylori*. In this Article, we demonstrate that bismuth drugs synergize with various antibiotics against *P. aeruginosa* by targeting iron homeostasis.

Results

Bismuth drugs show synergy with antibiotics against *P. aeruginosa*

Inspired by the success of bismuth and antibiotic-based triple or quadruple therapies for *H. pylori*[22], we investigated a similar combination for other bacterial infections. We tested the minimal inhibitory concentration (MIC) of bismuth subsalicylate (BSS) against World Health Organization priority pathogens[23], including Gram-negative pathogens *P. aeruginosa*, *Klebsiella pneumoniae*, *Acinetobacter baumannii*, *Escherichia coli*, *Salmonella enterica* and *Shigella flexneri* and the Gram-positive pathogens *Mycobacterium marinum*, *Streptococcus pneumoniae* and *Staphylococcus aureus*. The results showed that all bacteria were highly resistant to BSS (MIC > 1,024 μM). We then screened for potential synergy of BSS (16 μM) with 30 antibiotics. Surprisingly, BSS showed good to excellent synergy with all antibiotic classes against *P. aeruginosa* (PAO1), with a fractional inhibitory concentration (FIC) index (FICI) ranging from 0.018 to 0.256 and MIC reductions of 4- to 256-fold (Fig. 1 and Supplementary Table 1). BSS also showed modest synergy against some other Gram-negative bacteria (Fig. 1). The synergy was confirmed in three other *P. aeruginosa* strains. We further examined the synergy of four other bismuth drugs (bismuth citrate, colloidal bismuth subcitrate (CBS), bismuth gallate, bismuth nitrate) and five metal compounds with 55 antimicrobial agents against PAO1. The results showed that all bismuth drugs had strong synergistic effects with tetracyclines, macrolides, quinolones, rifamycins, chloramphenicol, certain β-lactams and other antibiotics. These effects were specific to bismuth ions, as they were absent with ligands alone. By contrast, silver and indium compounds showed limited synergy, primarily with aminoglycoside and tetracycline antibiotics, respectively (Extended Data Fig. 1 and Supplementary Table 2).

Using a checkerboard microdilution test, we found that a low concentration (4–8 μM) of BSS reduced the MICs of various antibiotics by 8- to 128-fold against PAO1, despite that BSS alone had an MIC above 1 mM (Extended Data Fig. 2). Weaker synergy was observed with tobramycin, cefepime or aztreonam (Extended Data Fig. 2). Given the primarily bacteriostatic nature of the synergistic drugs, we examined the biocidal action by time-killing assay. Most antibiotics alone could not kill the bacteria at the plateau phase, except for azithromycin (Extended Data Fig. 3)[24]. When combined with BSS, azithromycin rapidly killed bacteria even in the logarithmic growth phase (Extended Data Fig. 3a). Similar effects were observed with chloramphenicol, clarithromycin and telithromycin (Extended Data Fig. 3b–d). Although
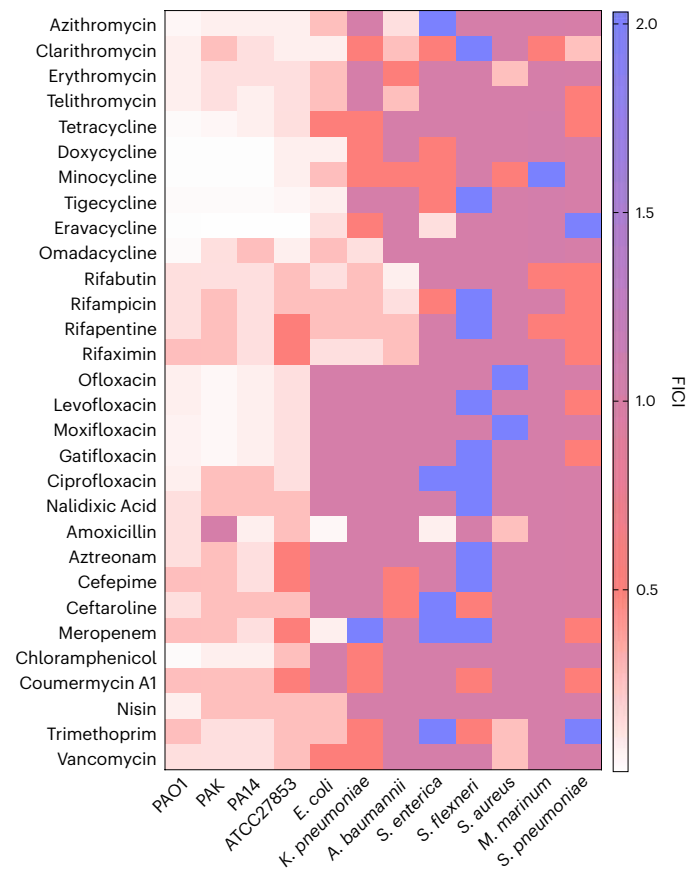

Fig. 1 | Bismuth enhances the antimicrobial activity of multiple antibiotics against *P. aeruginosa*. The heat map of the FICIs for the synergistic effects of BSS and antibiotics against *P. aeruginosa* (PAO1, PAK, PA14, ATCC27853) and other pathogens. A synergy is defined as a FICI ≤ 0.5.

P. aeruginosa is resistant to tetracycline antibiotics, including tigecycline and eravacycline (ERV), combining these antibiotics with BSS produced effective bactericidal effects (Extended Data Fig. 3e–i). BSS combined with rifampicin reduced cell viability by ~8 log$_{10}$ units (Extended Data Fig. 3j). BSS also notably enhanced the bactericidal activity of low concentrations of tobramycin, aztreonam and quinolones (ofloxacin, ciprofloxacin and moxifloxacin), reducing the bacterial population by over 8 log$_{10}$ units after 24 h (Extended Data Fig. 3k–o).

BSS disrupts iron homeostasis in *P. aeruginosa*

To understand the synergy of BSS with antibiotics, we conducted transcriptome analyses of PAO1 exposed to BSS (16 μM) for 30 min. BSS notably downregulated genes related to *P. aeruginosa* siderophore synthesis (*pvdA*, *pchABCD*), iron uptake receptor (*fpvA*, *chtA*, *fptA*, *piuA*, *fecA*) and the iron uptake central regulator *pvdS* (Fig. 2a, Supplementary Table 3). Reverse transcription-quantitative polymerase chain reaction (RT-qPCR) confirmed these results (Extended Data Fig. 4a). In accordance, BSS reduced pyoverdine (PVD) production without affecting bacterial growth (Fig. 2b), suggesting it disrupts iron homeostasis. To prove this, we quantitatively assessed the overall intracellular iron concentration upon the treatment with BSS by inductively coupled plasma mass spectrometry (ICP-MS). ICP-MS analysis showed BSS decreased intracellular iron and increased bismuth levels, indicating interference with iron uptake (Fig. 2c). Supplementing iron (FeCl$_3$) counteracted BSS's synergistic effects with ERV and other antibiotics, preventing *P. aeruginosa* killing (Extended Data Fig. 4b,c and Supplementary Fig. 1).

The host defends against pathogens by depriving them of iron[25]. *P. aeruginosa* uses siderophores such as PVD and pyochelin (PCH) to
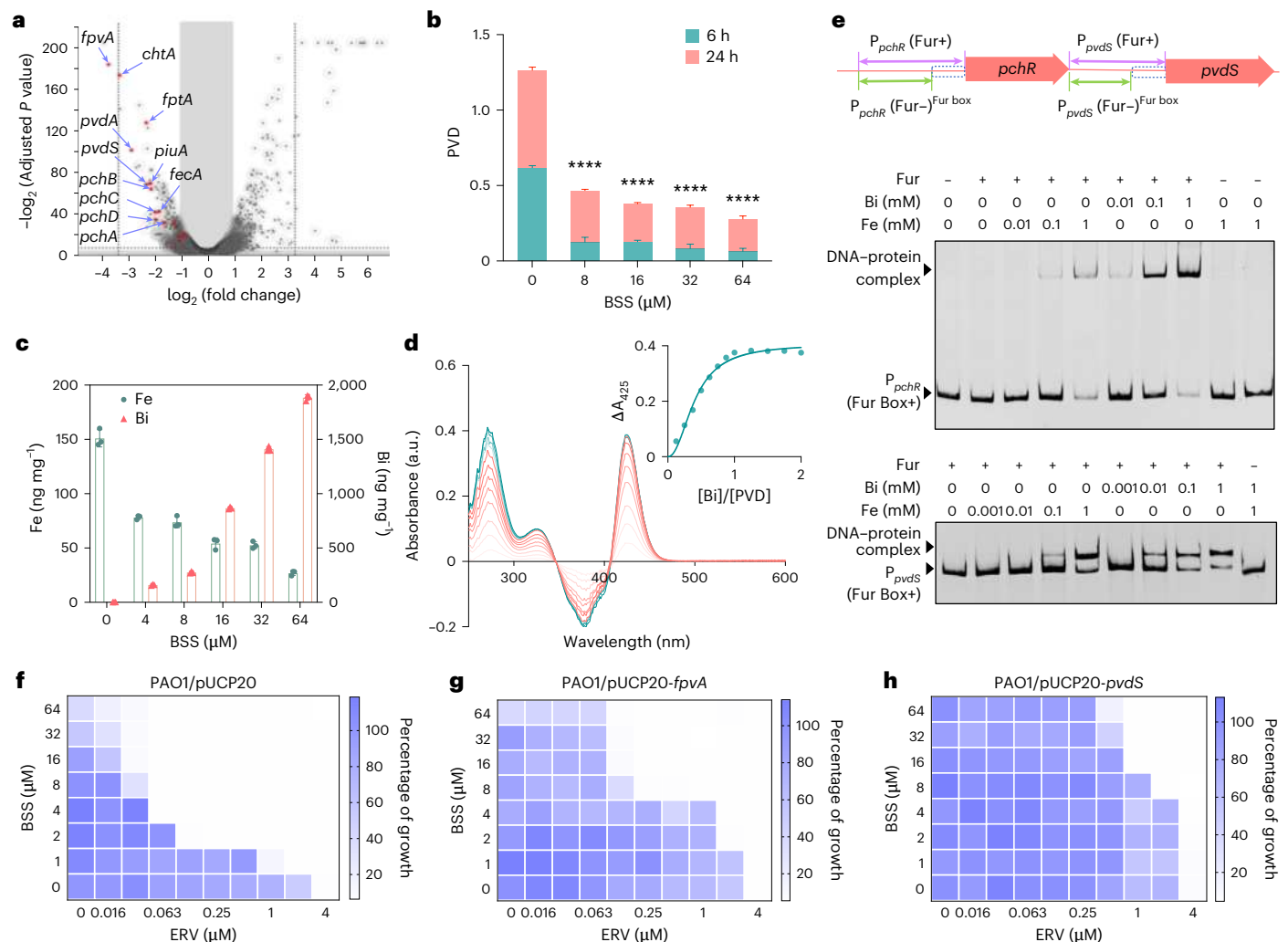
Fig. 2 | Bismuth disrupts the iron homeostasis of *P. aeruginosa*. a, Volcano plot analysis of the differential expressed genes in PAO1 after exposure to BSS for 30 min. The significantly changed iron uptake-related genes are shown in red. The data are presented as the mean of two biological replicates; two-sided *t*-test was used, and multiple testing correction was done using Benjamini–Hochberg procedure and given as adjusted *P* value. Plots in the shading indicate genes that are not significantly expressed. **b**, The relative amounts of PVD produced in PAO1 treated with different concentrations of BSS at different time points (OD$_{405}$/OD$_{600}$). **c**, Total iron and bismuth concentrations in the PAO1 cells treated with BSS for 4 h. **d**, Different UV–vis spectra of PVD upon addition of 0.125–2.000

molar equivalents of Bi(NTA). The inset shows the changes in absorbance at 425 nm (ΔA_{425}). **e**, The scheme shows the location of the DNA fragments by arrows. Binding of Fur to the *P. aeruginosa* Fur box (P$_{pvdS}$ and P$_{pchR}$, promoter of *pvdS* and *pchR*) depends on the presence of Bi or Fe. **f**–**h**, Heat maps show that overexpression of *fpvA* (**g**) or *pvdS* (**h**) antagonizes the synergy of bismuth with ERV, while the empty vector (**f**) does not affect the synergy. The data are presented as mean ± s.d. of three biological replicates for **b** and **c**; ****$P < 0.0001$ versus untreated sample by two-sided unpaired *t*-test. *P* values are 0.0000098, 0.0000001, 0.0000054 and 0.0000033.

acquire iron. Despite their high affinity for iron[26], our results show that bismuth interferes with these iron acquisition systems. Next, we explored whether bismuth directly interacts with these sidero-phores and enters the cells. Ultraviolet–visible (UV–vis) spectroscopy revealed that adding Bi(III) (as bismuth nitrilotriacetate, Bi(NTA) to PVD resulted in absorption bands at 325 and 425 nm, characteristic of bismuth ligand-to-metal charge transfer bands. The intensities of these bands increased and levelled off at a molar ratio of [Bi]/[PVD] ≈ 1, sug-gesting each PVD binds one Bi(III) (Fig. 2d). By fitting the titration curve with the Ryan–Weber nonlinear equation, the dissociation constant (K_d) was calculated to be 0.52 ± 0.15 μM, and the apparent dissociation constant (K_d') was 1.45 (±0.43) × 10^{-18} μM, considering Bi(III) and NTA binding affinity (log K_a = 17.55)[27]. MS confirmed this binding with a new peak at *m/z* 770.7782 (calculated mass-to-charge ratio 770.7779 for PVD1-Bi) (Extended Data Fig. 4d). Despite PVD having lower affinity for bismuth than iron ($K_d' \approx 10^{-26}$ μM)[28], considering the extremely low level of free iron in the physiological environment, bismuth can still

bind effectively to PVD, interfering with iron acquisition. Similarly, the binding of Bi to PCH was also confirmed by UV–vis spectroscopy (Extended Data Fig. 4e), with K_d and K_d' calculated to be 1.15 ± 0.43 μM and 3.24 (±1.20) × 10^{-18} μM, respectively.

The binding affinities of bismuth to these siderophores suggest bismuth might use *P. aeruginosa*'s iron acquisition system for internalization and accumulation. However, deleting the PVD synthesis gene (*pvdA*), the PCH synthesis gene (*pchD*) or ferripyover-dine primary receptor gene (*fpvA*) did not affect the synergy between BSS and ERV (Supplementary Fig. 2). Although intracellular bismuth decreased in the *ΔpvdA/ΔpchD* strain, a notable amount of bismuth still accumulated, indicating alternative uptake pathways (Extended Data Fig. 4f). It is worth noting that adding exogenous PVD antago-nized the BSS–ERV synergy, while PCH supplementation enhanced it (Supplementary Fig. 3).

In iron-limited conditions typical in infections sites, ferripyo-verdine uptake is facilitated by FpvA receptor, activating the sigma

factor PvdS and upregulating siderophore biosynthesis and receptor genes[29]. This process is repressed by the ferric uptake regulator (Fur) when the intracellular iron is sufficient. Under these conditions, Fe is bound to Fur, and the Fur–Fe complex can bind specific DNA motifs (Fur boxes) in the promoter region of target genes, repressing their expression. The repressed *pvdS*, involved in siderophore synthesis and receptor genes, suggests that bismuth mimics iron by binding to the Fur protein[30], thus inhibiting the expression of these genes. To test this hypothesis, we determined the binding capacity of Fur with its targets at different bismuth/iron concentrations via an electrophoretic mobility shift assay using the Fur box DNA sequence from the *pchR* and *pvdS* promoters. As shown in Fig. 2e, bismuth promoted Fur binding to its target DNA with higher affinity than iron (Fig. 2e and Supplementary Fig. 4). Furthermore, bismuth's synergy with ERV was reduced in bacteria overexpressing *fpvA* or *pvdS* but not with an empty vector (Fig. 2f–h). Collectively, our results indicate that bismuth impairs iron uptake by interacting with siderophores and Fur, leading to intracellular iron deprivation.

BSS inhibits the electron transport chain

As BSS caused iron deprivation in bacterial cells, we investigated its effect on the electron transport chain (ETC), where iron–sulfur cluster enzymes are essential. In aerobiosis, oxygen acts as the electron acceptor in the final ETC step, and the oxygen consumption rate reflects electron transport and respiration rates[31]. To assess BSS's impact on ETC activity in PAO1, we measured the time-dependent oxygen consumption rate using an oxygen-quenched fluorescent probe in PAO1 as well as in *nuoB* mutant strain. BSS treatment resulted in a dose-dependent reduction in fluorescent signal increase, indicating diminished ETC activity and reduced respiration. At 64 μM, BSS slowed down ETC activity similar to the *nuoB* mutant (Extended Data Fig. 5a). We observed a dose-dependent increase in intracellular reduced nicotinamide adenine dinucleotide (NADH) levels (Fig. 3a and Supplementary Fig. 5a), which should be oxidized to nicotinamide adenine dinucleotide (oxidized form) (NAD$^+$) in the ETC's first step by the NADH dehydrogenases, the richest Fe–S cluster enzymes in the ETC[32]. This suggests that BSS may interfere with this enzyme's function, possibly by disrupting the Fe–S cluster. To validate this hypothesis, we purified the *P. aeruginosa* membrane fractions containing NADH dehydrogenases before and after bismuth treatment. We observed a dose-dependent inhibition of NADH dehydrogenase by BSS (Fig. 3b and Extended Data Fig. 5b). *P. aeruginosa* has three NADH dehydrogenases: Nuo (high-iron complex), Nqr (single [2Fe–2S] cluster) and NdhII (no iron atoms). To investigate which enzyme was inhibited by BSS, we purified the membrane fractions from specific NADH dehydrogenase mutant strains and examined their NADH dehydrogenase activity in the presence of BSS. The *nuoB* mutant was not sensitive to BSS, while the *nqrA* and *ndh* mutants showed similar sensitivity to the wild-type strain (Extended Data Fig. 5c–f), although other NADH dehydrogenases might contribute to rapid NADH consumption in the *nuoB* mutant (Supplementary Fig. 5b). BSS lost its activity with the Nuo inhibitor rotenone but not with the Nqr inhibitor 2-heptyl-4-hydroxyquinoline-N-oxide (Supplementary Fig. 5c–e). This suggests that BSS likely inhibits Nuo NADH dehydrogenase activity by targeting the Fe–S cluster. Other Fe–S cluster enzymes in the ETC, such as succinate dehydrogenase (Sdh), might also be targeted by BSS. Attempts to study BSS's effect on Sdh using a *sdh* mutant strain were unsuccessful due to the enzyme essentiality[33]. However, a Sdh assay showed that BSS did not affect Sdh activity (Supplementary Fig. 5f). Compounds disrupting Fe–S clusters typically target proteins with exposed Fe–S clusters, such as aconitase in the 4Fe–4S dehydratase family. We tested aconitase activity after BSS treatment and found it was inhibited (Supplementary Fig. 5g). Consistently, bacteria cultured in M9 medium without isoleucine, leucine and valine did not grow under high BSS concentrations, but growth was improved with the addition of these amino acids (Supplementary Fig. 5h,i). This suggests

BSS might affect the Fe–S proteins involved in branched chain amino acids biosynthesis.

Transcriptomic analyses showed that the Fe–S biogenesis system Isc (PA3809–PA3815) is not upregulated, indicating that Bi(III) likely targets Fe–S cluster enzymes directly rather than affecting their biogenesis. This aligns with previous metalloproteomic studies that showed Bi(III) binds to Fe–S cluster enzymes in *H. pylori* including isocitrate dehydrogenase[34]. To verify that BSS disrupts Fe–S clusters and releases iron in *Pseudomonas*, we measured intracellular iron contents via the calcein-acetoxymethylester (calcein-AM) fluorescent probe[35]. The green fluorescence of calcein-AM is quenched by low-mass labile iron but not iron in large protein complexes. BSS treatment of PAO1 resulted in a dose-dependent increase in Fe release (Extended Data Fig. 5g). In M9 medium without iron, BSS treatment did not change fluorescence, but fluorescence was quenched with iron and PVD treatment (Extended Data Fig. 5h,i). Collectively, we demonstrate that BSS inhibits ETC activity, likely by specifically inhibiting Fe–S cluster enzymes such as Nuo NADH dehydrogenase in *P. aeruginosa*, disrupting iron–sulfur systems.

BSS induces the dissipation of the proton motive force

During electron transfer through the ETC, protons are pumped across the membrane, generating a proton gradient for ATP synthesis. Inhibiting the ETC dissipates the proton motive force (PMF), impairing ATP generation and the functionality of multidrug efflux pumps. To confirm BSS disrupts PMF, we measured changes in the cytosolic pH of PAO1 cells with or without BSS treatment using the 2′,7′-Bis-(2-carboxyethyl)-5-(and-6)-carboxy fluorescein acetoxymethyl ester (BCECF-AM) probe[36]. A dose-dependent decrease in BCECF-AM fluorescence indicated a reduction in ΔpH, showing that BSS disrupts ΔpH (Fig. 3c). Given that PMF is generated by two components, that is, the membrane potential, ΔΨ, and the pH gradient, we also measured ΔΨ directly using the membrane potential indicator dye 3,3′-diethyloxacarbocyanine iodide (DiOC2(3)) and observed the reduced red/green fluorescence ratios, indicating membrane potential disruption by BSS (Extended Data Fig. 6a). Consequently, intracellular ATP levels and efflux pump activity were reduced (Fig. 3d,e). In addition, we observed a synergistic effect of the efflux pump inhibitor PAβN with BSS (Fig. 3f), suggesting an alternative mechanism of action of bismuth on the efflux pumps. To further verify the inhibitory effect of BSS on the efflux pumps, we measured the intracellular bismuth content in the wild-type PAO1, with and without efflux pumps inhibitor phenylalanine-arginine β-naphthylamide (PAβN), and in efflux pumps mutant Δ*oprM/mexCD* strain. We found that intracellular bismuth initially accumulated rapidly in the wild-type bacterium and then gradually decreased (Extended Data Fig. 6b). By contrast, more bismuth was accumulated in the efflux pumps *oprM/mexCD* deleted strain or in PAO1 with PAβN (Fig. 3g). The impairment of the pumps by BSS resulted in a dose-dependent accumulation of antibiotics including not only evracycline and azithromycin but also other classes of antibiotics, for example, ofloxacin and chloramphenicol (Fig. 3h and Extended Data Fig. 6c–e). Furthermore, the inhibitory effect of BSS on the efflux pumps was also confirmed by neutralizing the effect of the efflux pump inhibitor PAβN (Fig. 3i and Supplementary Fig. 6), which showed a similar synergy with antibiotics as bismuth against *P. aeruginosa* (Supplementary Fig. 7). These results suggest that the bismuth concentration used is sufficient to block the efflux pumps, allowing antibiotics to reach bactericidal levels inside the cell. In the case of the Δ*oprM*/Δ*mexCD* mutant, this concentration was achieved even at lower bismuth concentrations (2 μM), highlighting the role of efflux pumps in bismuth detoxification (Extended Data Fig. 7). Overall, we demonstrate that bismuth potentiates antibiotics by inhibiting ETC activity possibly via targeting key Fe–S cluster enzymes such as Nuo NADH dehydrogenase. This leads to PMF dissipation and efflux pumps impairment, resulting in intracellular antibiotics accumulation.
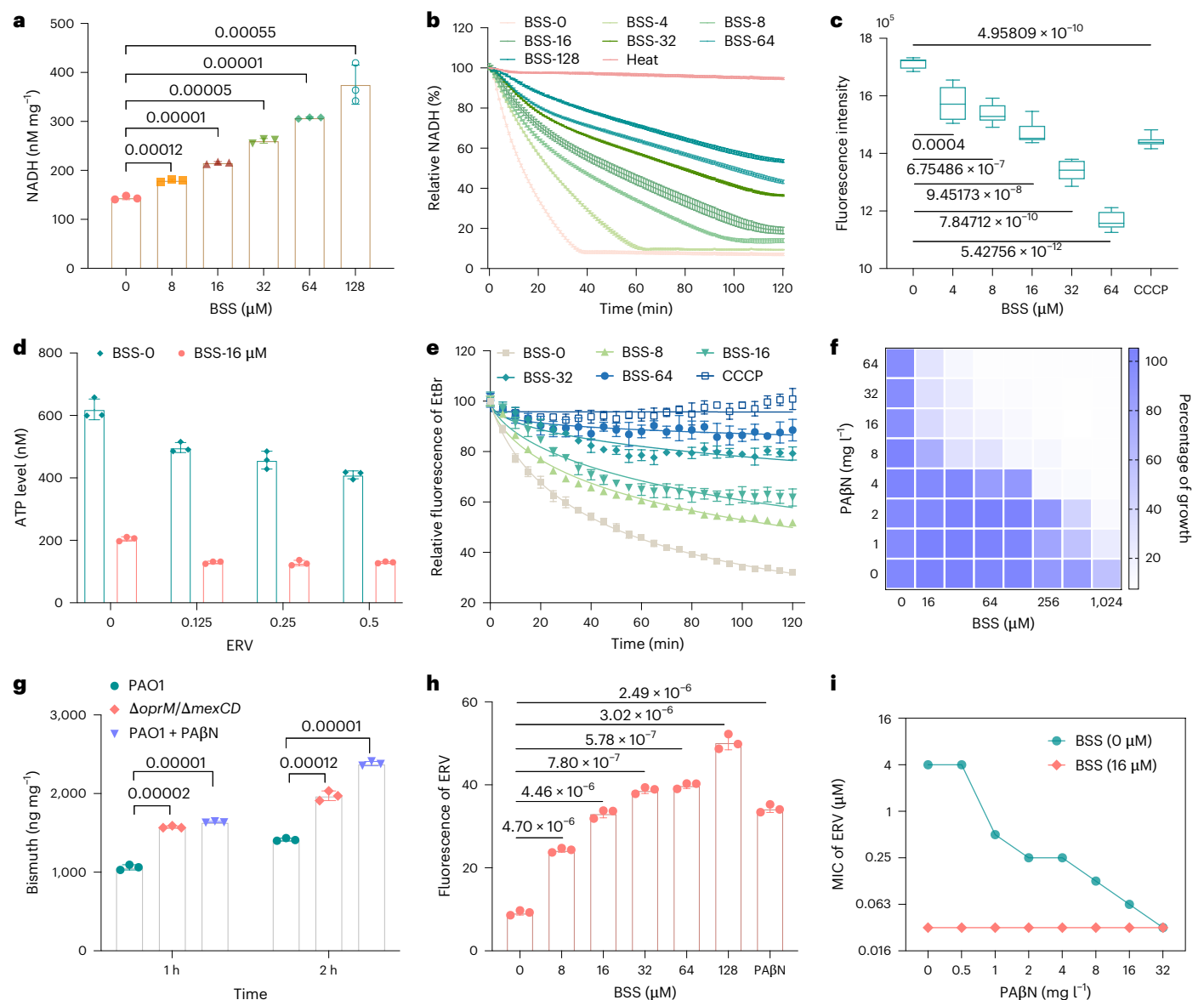
Fig. 3 | Bismuth impairs the activity of the ETC, inhibits efflux pumps, and promotes intracellular antibiotic accumulation in *P. aeruginosa*.
a, Intracellular NADH concentration in PAO1 cells treated with BSS. **b**, BSS dose-dependent inhibition on the activity of NADH dehydrogenase. The bacterial inner membrane was collected and treated with different concentrations of BSS (μM) for 2 h, then the membrane-bound NADH–quinone oxidoreductase activity was measured. **c**, BSS dose-dependent decrease in the fluorescence signals reflects the increased PMF disruption. CCCP was used as a positive control. Whisker plots show the ranges from the minimum to the maximum. The boundaries of the box indicate the 25th percentile and the 75th percentile. Within each box, horizontal lines denote median values of six biological replicates. **d**, The intracellular ATP levels of *P. aeruginosa* under the indicated treatment for 1 h. **e**, BSS (μM) dose-dependent inhibition on EtBr efflux. CCCP was used as a positive control. **f**, Representative heat plot of microdilution checkerboard assay for the combination of the efflux pumps inhibitor PAβN and BSS against PAO1. **g**, Intracellular bismuth concentration in the PAO1 cells or in the presence of 16 mg ml^{-1} efflux pumps inhibitor PAβN or *oprM/mexCD* deletion strains treated with 16 μM BSS. **h**, Intracellular BSS dosage-related accumulation of ERV. PAβN (16 mg ml^{-1}) was used as a positive control. **i**, BSS antagonizes the synergistic effects of the efflux pumps inhibitor PAβN and ERV. For **a**, **b**, **d**, **e**, **g** and **h**, the data are presented as mean ± s.e.m. of three biological replicates. For **a**, **c**, **g** and **h**, *P* values were determined using two-sided unpaired *t*-test.

BSS prevents the bacterial evolution of antibiotics resistance

Preventing the evolutionary selection of antimicrobial-resistant bacteria is crucial to reducing antibiotic resistance[13]. To understand BSS's effects on developing antibiotic resistance, we performed serial passages of PAO1 with sub-MIC (0.25 × MIC) of ERV and ofloxacin with and without BSS (16 μM) for 25 days. Sequential passaging of antibiotics alone for 25 days resulted in 32- and 64-fold increases in their MICs (Fig. 4a,b). By contrast, co-administration of BSS with antibiotics resulted in only 2-fold increases in their MICs (Fig. 4a,b), suggesting that BSS prevented the development of high-level resistance. We

subsequently examined the MICs of three selected resistant strains to other antibiotics from the same group with and without BSS. As expected, the MICs notably increased for the resistant strains. Whole genome sequencing showed that all ofloxacin-resistant strains contained mutations in the quinolone target GyrAB and the efflux pump MexCD repressor NfxB (Supplementary Table 4). Conversely, all the ERV-resistant strains had mutations in the ribosomal protein RpsJ known to confer high resistance to tetracyclines in other bacteria (Supplementary Table 4)[37]. It is worth noting that the MICs of these quinolone/tetracycline-resistant strains were notably reduced in the
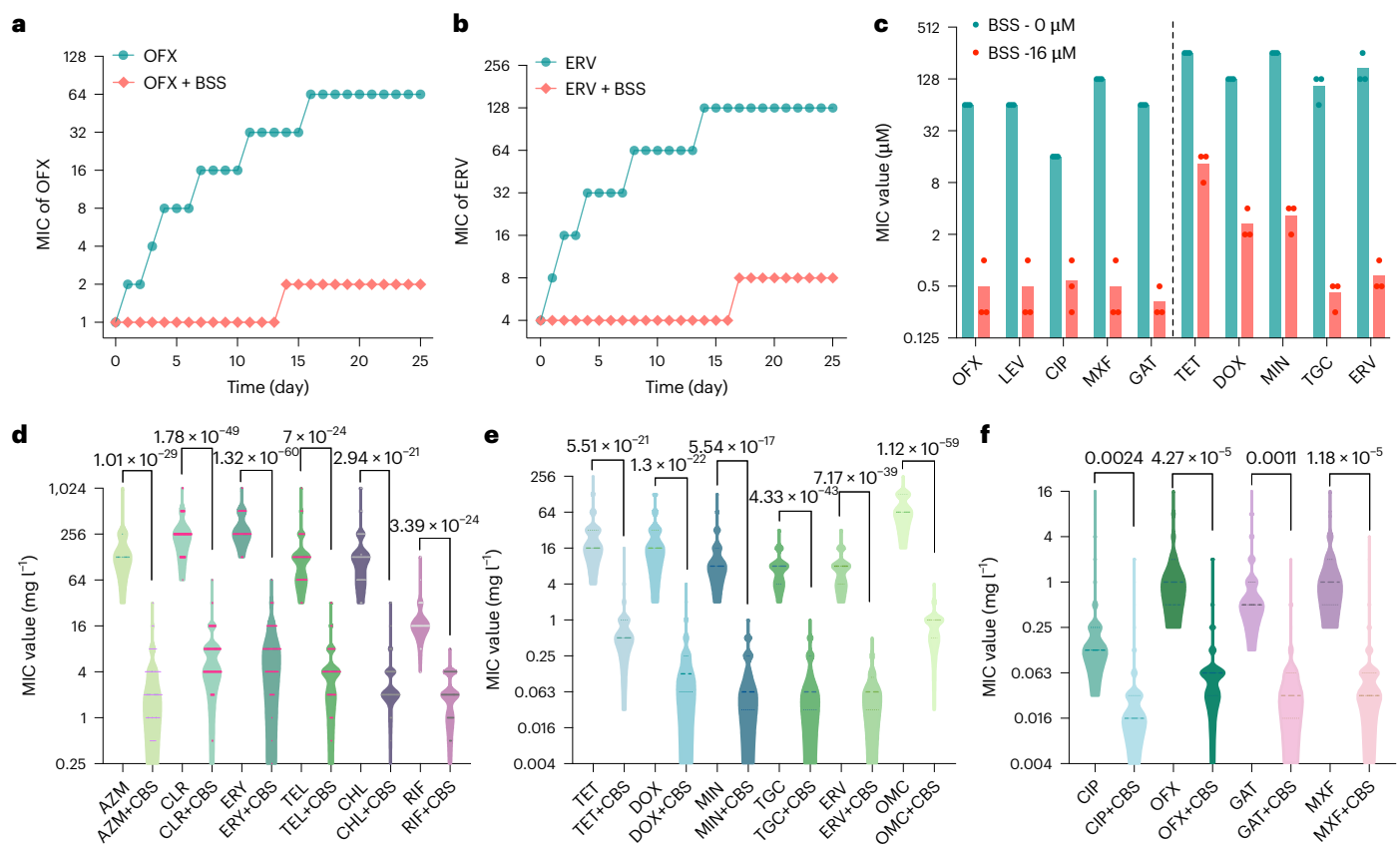
Fig. 4 | Bismuth prevents the evolution of antibiotics-elicited resistance and enhances the activities of antibiotics against clinical isolates. a,b, Resistance acquisition curves during serial passage with the subinhibitory concentration of ofloxacin (**a**) and ERV (**b**) or their combination with BSS against PAO1, showing that BSS thwarts the resistant evolution of PAO1 to ofloxacin and ERV in vitro. The tests were performed in triplicate, and all the data are presented as the mean of the median. **c**, The MICs of tetracycline or quinolone antibiotics for the resistant strains in the absence or presence of 16 μM BSS. **d–f**, Susceptibility testing shows CBS (8 mg l^{-1}) enhances the efficacy of multiple antibiotics against 124 clinically relevant *P. aeruginosa* strains. The antibiotics used are macrolides (azithromycin (AZM), clarithromycin (CLR), erythromycin (ERY), telithromycin (TEL)), chloramphenicol (CHL) and rifampicin (RIF) (**d**), tetracyclines (tetracycline (TET), doxycycline (DOX), minocycline (MIN), tigecycline (TGC), eravacycline (ERV), omadacycline (OMC)) (**e**) and quinolones (ciprofloxacin (CIP), ofloxacin (OFX), gatifloxacin (GAT) and moxifloxacin (MXF)) (**f**) on 124 clinically relevant *P. aeruginosa* strains. Violin plots show the kernel probability density of the data, which ranges from the minimum to the maximum observed MIC$_{90}$ value (*n* = 124). The dotted lines represent the median and quartiles of the data; the results were obtained from two biological replicates of each bacterial isolate. *P* values were determined using two-sided unpaired *t*-test.

presence of BSS (Fig. 4c), suggesting that bismuth can overcome antibiotic resistance regardless of the resistance mechanism.

Bismuth increases the activity of antibiotics in complex matrices

Chronic *P. aeruginosa* infections due to biofilm formation pose clinical challenges[38]. Therefore, we evaluated whether bismuth could enhance antibiotic control of biofilms. While exponentially growing PAO1 is resistant to azithromycin, biofilm-forming cells are sensitive[24]. As depicted in Extended Data Fig. 8, biofilm bacteria were notably susceptible to azithromycin even at sub-MIC concentrations. In this case, introducing BSS only marginally augmented the killing efficacy of azithromycin against biofilm-associated bacterial cells. However, for antibiotics with negligible or marginal effectiveness alone, combining them with BSS enhanced their killing efficacy against biofilm-associated bacterial cells (Extended Data Fig. 8). Moreover, we examined the antimicrobial efficacy of bismuth drugs, antibiotics and their combination in an ex vivo bacteraemia model. The combination showed notably better bactericidal effects, with over 3 log$_{10}$ reductions of colony-forming units (c.f.u.) in the blood, while bismuth or antibiotics alone could not control the infection (Extended Data Fig. 9a). It is worth noting that one dose of the combination therapy controlled the infection for over 24 h, even at low concentration (Extended Data Fig. 9b).

Bismuth enhances antibiotics efficacy against clinical isolates

To assess the clinical applicability of combining bismuth drugs and antibiotics, we tested 8 mg l^{-1} of CBS with antibiotics against 124 *P. aeruginosa* clinical isolates. The MICs of macrolides were reduced by 32- to 64-fold (Fig. 4d and Supplementary Table 5) and tetracycline-related antibiotics by 32- to 128-fold (Fig. 4e and Supplementary Table 6). Similarly, the MICs of chloramphenicol, rifampicin and quinolone-related antibiotics were notably reduced (Fig. 4d,f and Supplementary Tables 5 and 7).

Bismuth does not show toxicity after pulmonary delivery to mice

Unlike other heavy metals, bismuth drugs have negligible toxicity in the human body, due to glutathione and multidrug resistance protein-mediated self-propelled disposal[39]. No cytotoxicity in human lung epithelial or embryonic kidney cells, nor haemolytic activity on human erythrocytes, was observed even at very high concentrations of bismuth (Extended Data Fig. 10a–c).

Considering *P. aeruginosa* often causes lung infections, we studied bismuth toxicity in two mouse models (BALB/c and C57BL/6) via intranasal administration of CBS. No acute toxicity signs were observed at 100 mg kg^{-1} or 300 mg kg^{-1} (three dosages) in C57BL/6 mice, and lung tissue showed no pathological changes (Extended Data Fig. 10d).
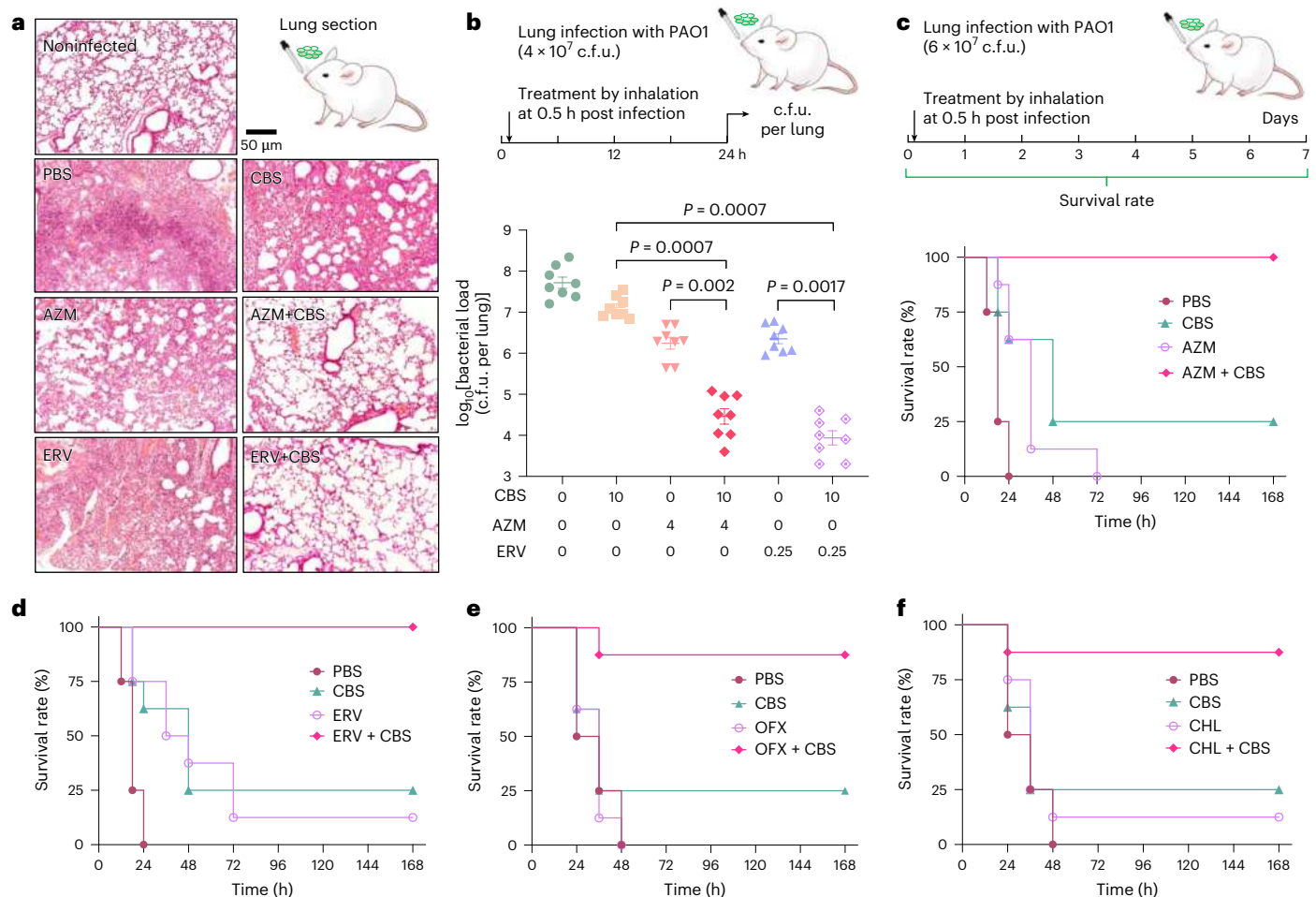
Fig. 5 | Bismuth enhances the efficacy of antibiotics against *P. aeruginosa* in vivo. a, Haematoxylin and eosin staining of the mouse lungs under different treatments 24 h post infection. **b**, Bacterial load in the mouse lung infection model (*n* = 8). The bacterial load in the lungs of mice infected with a sub-lethal dose of *P. aeruginosa* decreases notably after a single dose treatment with the drug combinations. *P* values were determined using two-sided unpaired *t*-test.

The data are presented as means ± s.e.m. **c–f**, Survival curves showing the efficacies of the co-therapy in a mouse acute pneumonia model (*n* = 8). Increased survival rates of mice over 7 days challenging by a lethal dose of *P. aeruginosa* were observed in the mice treated with CBS (10 mg kg⁻¹) together with antibiotics compared with the monotherapy of AZM (2 mg kg⁻¹, **c**), ERV (0.25 mg kg⁻¹, **d**), OFX (1 mg kg⁻¹, **e**) or CHL (2 mg kg⁻¹, **f**).

For BALB/c mice, all survived at a 200 mg kg^{-1} dosage, indicating a maximal tolerance dose higher than 200 mg kg^{-1} (Extended Data Fig. 10e). To investigate bismuth's lung delivery and excretion, we analysed organ distribution after intranasal administration of 100 mg kg^{-1} CBS. As shown in Extended Data Fig. 10f, bismuth concentration in the lung decreased over time, with about 2% remaining at 24 h, indicating no lung accumulation. No accumulation was observed after administering CBS (100 mg kg^{-1}) for 3 consecutive days. A similar bismuth concentration was observed in the lungs after 72 h. At the same time, we observed accumulation of bismuth in the kidney, with much lower levels in the heart, spleen and liver, suggesting kidney excretion (Extended Data Fig. 10f).

Bismuth enhances antibiotics efficacy against *P. aeruginosa* in vivo

We finally investigated the effectiveness of combined bismuth drug and antibiotic therapy in a mouse acute pneumonia model. Female BALB/c mice were infected by a sub-lethal dose of PAO1 via inhalation. After half an hour, the infected mice received a single intratracheal dose of either vehicle control, antibiotics, CBS monotherapy or combination therapy. Histological lung sections confirmed reduced inflammation and tissue injury with the drug combinations (Fig. 5a). We observed that the combinations of CBS (10 mg kg^{-1}) with azithromycin (4 mg kg^{-1}) or

ERV (0.25 mg kg^{-1}) resulted in over 2–3 log$_{10}$ reductions in lungs c.f.u. compared to the monotherapy at 24 h post infection (Fig. 5b). In a lethal *P. aeruginosa* infection model, CBS (10 mg kg^{-1}) with azithromycin (2 mg kg^{-1}) or ERV (0.25 mg kg^{-1}) led to 100% survival, while the combinations of CBS with ofloxacin (1 mg kg^{-1}) or chloramphenicol (2 mg kg^{-1}) increased survival rates of mice to 87.5% over 7 days (Fig. 5c–f). With monotherapies, azithromycin and ofloxacin failed to protect any of the mice within 72 h, while ERV and chloramphenicol each rescued 1 out of the 8 mice by the experiment's end (Fig. 5c–f). Surprisingly, although CBS alone has poor in vitro antibacterial activity against *P. aeruginosa* (MIC > 1,024 µM), a single dose of 10 mg kg^{-1} CBS rescued 2 out of the 8 mice, resulting in a 25% survival (Fig. 5c–f). As bismuth can directly target PVD, essential for in vivo iron chelating and expression of virulence factors in *P. aeruginosa*[29,40], this anti-virulence effect may explain the in vivo efficacy at a low dose. Overall, we demonstrate the high potential of bismuth drugs as antibiotic adjuvants to potentiate antibiotics against *P. aeruginosa* in vivo.

Discussion

The emergence of antimicrobial-resistant bacterial strains highlights the limitations of current single-targeted drug design. Alternative strategies are urgently needed to tackle AMR, the silent pandemic. Using antimicrobial metals alone or with antibiotics is a promising

approach to address this issue[12,41–44]. This study reveals strong synergy between a bismuth drug and multiple antibiotic classes against *P. aeruginosa*. It is worth noting that the combination therapy enhanced survival rates in a mouse infection model with a well-tolerated safety profile. Our in-depth mechanistic studies reveal that bismuth potentiates antibiotics by binding siderophores and the Fur, disrupting iron homeostasis. The contest for iron between the host and the pathogen is crucial for pathogen survival and disease progression. Most pathogens use multiple iron uptake systems to compete with the host for iron including producing high-affinity siderophores to capture iron from the host iron-binding proteins[45]. In *Pseudomonas*, 6% of genes are iron-responsive[46], indicating the importance of iron for this pathogen. Targeting bacterial iron acquisition, such as with the 'Trojan horse' strategy, is a promising approach against infection[41,47]. This strategy is successful, evidenced by the approval of cefiderocol, the first in-use siderophore-conjugated antibiotic.

Bismuth causes intracellular iron deprivation, impairing the ETC and dissipating the PMF. This inhibits ATP generation and compromises multi-drug efflux pumps, leading to increased antibiotic accumulation inside cells and enhanced susceptibility of *P. aeruginosa* to multiple antibiotics (Extended Data Fig. 10g). This mode of action of bismuth drugs makes them potentially promising antibiotic adjuvants for treating *P. aeruginosa* infections.

A battery of Fe−S clusters containing enzymes are involved in ETC functions[48]. In this study, we observed intracellular NADH accumulation in BSS-treated bacteria, suggesting BSS disrupted NADH dehydrogenases, the richest Fe−S cluster enzymes in the ETC[32]. This was confirmed by BSS losing activity in the presence of the Nuo NADH dehydrogenase inhibitor rotenone. However, the precise mechanism of how bismuth targets Fe−S clusters at the enzymatic level requires further study. Based on our extensive knowledge of bismuth biocoordination chemistry, Bi(III) resembles Fe(III) and Zn(II) and binds to iron-binding and zinc finger proteins[17,49]. The unique thiol-philic nature of Bi(III) has rendered diversified medicinal application of bismuth drugs being revealed[20,49]. Our previous metalloproteomic study revealed that Bi(III) binds to Fe−S cluster enzymes[16]. Therefore, BSS functionally disrupting Fe−S cluster containing enzymes is likely due to the binding of Bi(III) to the Fe−S clusters, resulting in the release of iron. Whether this is the case may warrant further studies in future.

Bismuth drugs, typically used orally for *H. pylori* and as salves for wound infections, have also been shown to suppress severe acute respiratory syndrome coronavirus 2 replication in a hamster model, alone or with N-acetyl cysteine[49,50]. Their low toxicity is attributed to low bioavailability[51], but enhanced absorption with N-acetyl cysteine does not cause apparent toxicity[50], suggesting their use beyond local infections such as *H. pylori*. Indeed, the intratracheal administration of high-dose CBS to mice showed no observable toxicity. Notably, combination therapy showed potent antimicrobial efficacy against *P. aeruginosa* in mouse lung infection models, with almost 100% survival rates for certain combinations. The high potency and safety profile indicate high translational potential of the combination therapy for treating drug-resistant *P. aeruginosa* infections.

Methods
Bacterial strains, primers and antibiotics
The bacterial strains and primers (synthesized by BGI genomics) used in this study are listed in Supplementary Table 8. Bacteria were cultured in cation-adjusted Muller−Hinton broth (CAMHB) or Luria−Bertani (LB) broth medium at 37 °C with agitation at 200 r.p.m. Bismuth potassium citrate was purchased from TCI. All other chemicals and antibiotics were purchased from Sigma-Aldrich or MedChemExpress unless otherwise stated.

Briefly, to construct the gene deletion mutant in *P. aeruginosa*, around 1,000 bp fragments that are upstream and downstream of the gene coding region were amplified by PCR using the PAO1 chromosome

as the template, and the primers are listed in Supplementary Table 8. The fragments were cloned into the plasmid pEX18TC by USER cloning (New England Biolabs). The plasmid was transfomed into *E. coli* S17 and then transferred into *P. aeruginosa* by conjugation. Single-crossover mutants were selected on 50 mg l^{-1} tetracycline and 50 mg l^{-1} kanamycin (to kill the *E. coli* donor strain), and double-crossover mutants were selected by growth on LB plates containing 7.5% sucrose.

MIC determination and synergy test
The MIC values were determined in triplicate using standard broth micro-dilution following Clinical and Laboratory Standards Institute recommendations. Briefly, the drugs were twofold diluted in CAMHB and then mixed with an equal volume of bacterial suspension in a 96-well microlitre plate, resulting in a final bacterial concentration of 5×10^5 c.f.u. ml^{-1}. The MIC values were defined as no visible bacterial growth under the lowest concentration of antibiotics after overnight incubation at 37 °C. A standard checkerboard broth micro-dilution test was carried out to test the synergistic effects of the combined antibacterial agents. When required, FeCl$_3$, PVD, PCH or efflux pump inhibitor PAβN was added into the medium to assess the effect on the synergy between bismuth and antibiotics. For the screening, all the tests were performed in triplicate. For the checkerboard assay, the experiments were performed three times.

The FICI was calculated according to the previously described formula FICI = FIC$_a$ + FIC$_b$ = MIC$_{ab}$/MIC$_a$ + MIC$_{ba}$/MIC$_b$. The FICI was interpreted according to European Committee on Antimicrobial Susceptibility Testing as follows: antagonistic, FICI ≥ 2; indifferent, 1 < FICI < 2; additive, 0.5 < FICI ≤ 1; synergistic, FICI ≤ 0.5. For the FICI calculations, twice the highest concentration tested was used in the cases where the MIC was not reached.

Time-dependent killing curve
An overnight culture of PAO1 was diluted 1:100 into fresh CAMHB and incubated for 3 h at 37 °C under continuous shaking to the late log phase (optical density at 600 nm (OD$_{600}$) = 0.4−0.6). Then, the cells were challenged by either antibiotic or BSS (16 μM) alone or their combination. At the indicated time points, the samples were decimal serially diluted in PBS. About 10 μl of the dilutions were spotted on LB agar, and colony counts were determined after incubating overnight at 37 °C. All experiments were performed with three biological replicates.

PVD quantification assay
An overnight culture of PAO1 was diluted 1:100 into fresh casamino acid medium (0.5% casamino acids, 0.1 mM MgSO$_4$, 7 mM potassium phosphate buffer, pH 7.0). At given time points, the PVD from culture supernatants was measured by absorbance at 405 nm, normalized by the cell density of bacterial cultures (OD$_{600}$).

Intracellular iron and bismuth assay
Intracellular iron and bismuth were measured by ICP-MS. An overnight culture of PAO1 was diluted 1:100 into fresh CAMHB and incubated for 3 h at 37 °C under continuous shaking to the late log phase (OD$_{600}$ = 0.4−0.6). Then, the cells were treated with the indicated concentration of BSS and incubated for 4 h at 37 °C under continuous shaking. The cells were collected by centrifugation and washed three times with 20 mM Tris−HCl pH 7.2 buffer. The bacterial cells were lysed by sonication. Bacterial lysates were supplemented with 68% HNO$_3$ to a final concentration of 5% and incubated at 65 °C overnight. The dissolved samples were centrifuged and diluted for the quantification of metals by ICP-MS (Agilent 7500a, Agilent Technologies). Metal quantifications were done in triplicate, and average values were used.

Cellular iron release
An overnight culture of PAO1 was diluted 1:100 into fresh CAMHB medium and allowed to grow at 37 °C until it reached the late log phase

(OD_{600} = 0.4–0.6). Subsequently, calcein-AM was added to the culture at a final concentration of 20 μM and incubated for 60 min at room temperature under conditions shielded from light. The bacterial cells were then subjected to three washes with PBS buffer and resuspended in fresh M9 medium containing the specified concentrations of BSS and further incubated for an additional hour at 37 °C under conditions protected from light. The cells were subsequently transferred to a 96-well plate, and the fluorescence intensity was measured using a Multi-Mode Microplate Reader (SpectraMax iD3, Molecular Devices, LLC) with excitation at 492 nm and emission at 535 nm.

Purification of PVD and PCH

P. aeruginosa (PAO1) cells were cultured overnight in succinate medium (K_2HPO_4, 6 g l^{-1}; KH_2PO_4, 3 g l^{-1}; $(NH_4)_2PO_4$, 1 g l^{-1}, $MgSO_4$, 0.2 g l^{-1}; succinic acid, 4 g l^{-1} and NaOH 1.1 g l^{-1}, pH = 7.0) and then diluted by 1:100 in the same medium. Cells were grown at 30 °C under continuous shaking for 48 h. The supernatant was collected after centrifugation (8,000 g, 4 °C for 30 min) and filtration through a 0.22 μm filter. For the PVD, the supernatant was loaded to a C18 reverse-phase SepPak column and sequentially washed with 10 ml of H_2O, 10 ml of 20% acetonitrile and 10 ml 80% of acetonitrile. The 20% acetonitrile solution was lyophilized to obtain crude PVD extracts. The crude extracts were dissolved in Milli-Q water filtered with a 0.22 μm filter and then subjected to a reverse high-performance liquid chromatography equipped with a 3.6 μ XB-C18 250 × 4.6 mm column for purification. A UV detector set at a wavelength of 280 nm was used to monitor the compound elution.

For the PCH, the supernatant from the bacterial culture was first acidified by the addition of solid citric acid to reach a pH of 3. The acidified supernatant was then subjected to two rounds of extraction with methylene chloride. The organic phase was carefully separated and collected, and any residual water was removed by adding $MgSO_4$. Next, the desiccant was filtered with a sintered glass funnel over a vacuum flask, and the solvent was evaporated under reduced pressure. The crude extracts were dissolved in 10% methanol and then purified by high-performance liquid chromatography. A UV detector set at a wavelength of 254 nm was used to monitor the compound elution.

UV–vis spectroscopy

UV–vis spectra were collected on a Varian Cary 50 spectrophotometer at a rate of 360 nm min^{-1} using a 1 cm quartz cuvette at ambient temperature. Aliquots of 2 mM Bi(NTA) stock solution were stepwise titrated into a PVD sample (100 μM) or PCH sample (50 μM) in a titration buffer (10 mM 4-(2-hydroxyethyl)-1-piperazineethanesulfonic acid (HEPES), 50 mM NaCl at pH 6.8), and UV–vis spectra were recorded in a range of 220–800 nm. Binding of Bi(III) to PVD was monitored by the increase in absorption at 325 nm and 425 nm. The binding of Bi(III) to PCH was monitored by the increase in absorption at 360 nm. The UV titration curve was fitted to the Ryan–Weber nonlinear equation.

$$I = \frac{I_{max}}{2C_p}\left[(K_d + C_m + C_p) - \sqrt{(K_d + C_m + C_p)^2 - 4C_m C_p}\right]$$

where I stands for UV absorbance intensity; I_{max} stands for maximal UV absorbance; C_p and C_m refer to the total concentrations of PVD and bismuth, respectively; K_d is the dissociation constant. The dissociation constant of Bi(III) from PVD was derived by $K_d' = K_d/K_a$, where K_d is the dissociation constant of Bi(NTA) from PVD determined from Ryan–Weber nonlinear fitting and K_a is the formation constant of Bi(NTA) with log K_a of 17.55.

Fur protein expression and purification

To express the Fur protein, the *fur* gene was amplified by PCR using the PAO1 chromosome as the template and primers as listed in Supplementary Table 8. The fragments were cloned into plasmid pET28a. The resulting plasmid was transferred into *E. coli* BL21(DE3). The BL21(DE3)

cells harbouring pET28a-*fur* plasmids were cultured overnight and then diluted by 1:100 to fresh LB medium supplemented with 50 μg ml^{-1} kanamycin. Cells were grown (37 °C and 200 r.p.m.) to OD_{600} of 0.4–0.6 and then induced by 1 mM β-D-thiogalactoside, and the bacteria were further incubated at 18 °C for 20 h. The bacteria were collected by centrifugation (8,000 g, 4 °C for 30 min), and the cell pellets were resuspended with a lysis buffer (50 mM Tris, 300 mM NaCl, 10% glycerol pH = 7.5) and sonicated. The lysates were centrifuged (12,000 g, 4 °C for 30 min), and the supernatant was incubated with the Ni(NTA) for 2 h at 4 °C and then washed three times with the lysis buffer with 20 mM imidazole. The Fur protein was eluted with 300 mM imidazole in the same buffer. The protein concentrations were quantified by a bicinchoninic acid (BCA) assay kit.

Electrophoretic mobility shift assay

DNA fragments (200 ng) were incubated with 1 μM purified recombinant Fur protein at 37 °C for 30 min in a 20 μl reaction mix (10 mM Tris–HCl, pH 7.6, 4% glycerol, 100 mM NaCl, 10 mM β-mercaptoethanol) including the indicated concentration of BSS or $FeSO_4$. Next, samples were loaded onto a 6% native polyacrylamide gel in 0.5× Tris–borate–EDTA buffer that was pre-run for 1 h and then run at 100 V for 2 h on ice. The gel was stained in 0.5× Tris–borate–EDTA containing ethidium bromide (EtBr) for 10 min, and bands were visualized with a molecular imager ChemiDoc XRS$^+$ (Bio-Rad).

Oxygen consumption assay

Bacterial oxygen consumption was measured using an extracellular oxygen consumption assay kit (Abcam, ab197243). An overnight culture of PAO1 was diluted 1:100 into fresh CAMHB medium and grown at 37 °C to the late log phase (OD_{600} = 0.4–0.6). The bacteria were treated with the indicated concentration of BSS for 2 h and then adjusted to 1×10^8 c.f.u. ml^{-1} in a fresh CAMHB medium containing the indicated concentration of BSS. About 150 μl of the bacterial resuspension was transferred to each well of a black 96-well plate containing 10 μl of O_2 consumption reagent. Each well was sealed with 50 μl mineral oil provided by the kit to isolate the air. The fluorescence signal was monitored at excitation/emission of 380/650 nm every 1 min for 30 min with a luminometer (Varioskan Flash; Thermo Scientific). All the tests were performed in triplicate.

Bacterial NADH level assay

Bacteria were cultured in a fresh CAMHB medium at 37 °C to an OD_{600} of 0.4–0.6. Then the bacteria were treated with the indicated concentration of BSS for 1 h. Following the treatment, 1.5 ml of the cell culture was collected via centrifugation and subsequently washed three times using a 20 mM Tris–HCl buffer at pH 7.2. The bacterial cells were then lysed via sonication. To determine the total protein concentration within the bacterial lysate, BCA analysis was conducted for calibration. In addition, 2 ml of culture was removed and immediately mixed with 8 ml ice-cold 100% methanol followed by centrifugation at 4,000 g for 15 min at 4 °C to obtain a cell pellet. The pellet was reconstituted in 0.2 M NaOH for the purpose of NADH extraction. This mixture was incubated at 52 °C for 10 min, followed by a subsequent incubation on ice for an additional 5 min. To neutralize the NaOH, 0.2 M HCl was added to the mixture, and gentle vortex mixing was used at low speed. The resulting mixture was then subjected to centrifugation for 15 min at 15,000 g and 4 °C. The supernatant was collected for NADH measurement. Total bacterial protein concentrations were quantified by BCA assay.

NAD(H) concentrations were measured using an enzyme cycling assay in a 96-well microtiter plate. Reagent master mix containing 2 volumes of 1 M bicine (pH 8.0), 1 volume of 100% ethanol, 1 volume of 40 mM EDTA (pH 8.0), 1 volume of 4.2 mM thiazolyl blue, 2 volumes of 16 mM phenazine ethosulfate and 1 volume of distilled water (dH2O) was prepared. Aliquots (30 μl) of NADH extracts were added

to individual wells of a 96-well microtiter plate, and reagent master mix (160 µl) was added and vigorously mixed (200 r.p.m., 3 s) followed by static incubation for 10 min in the microplate reader at 30 °C. Then, a solution of alcohol dehydrogenase (1 mg ml^{-1} in 0.1 M bicine) was added, followed by vigorous mixing (200 r.p.m., 1 s). The absorbance at 570 nm was then recorded every 30 s for 30 min, with vigorous shaking (200 r.p.m., 1 s) before each reading. The slopes of absorbance against time were calculated for NADH and were then used to calculate the concentration in the sample by fitting the standard curve prepared using the standard NADH sample.

Resazurin assay

The bacteria were cultured in the CA-MHB medium at 37 °C to an OD$_{600}$ of 1. BSS was added into the medium at the indicated concentrations. Resazurin was added at a final concentration of 0.1 mg ml^{-1}. Fluorescence resorufin was monitored at an excitation/emission wavelength of 550/590 nm every 10 min throughout 4 h with a spectrophotometer (Varioskan Flash; Thermo Scientific). All the tests were performed in triplicate.

Inner membrane preparation

P. aeruginosa PAO1 cells were grown in CAMHB medium overnight at 37 °C to obtain approximately 1–3 g wet weight of cells. For the in vivo test, overnight cultured PAO1 cells were treated with the indicated concentrations of BSS for 2 h, and then cells were collected by centrifugation and washed three times with sterile saline. To prepare spheroplasts, the cells were resuspended in 30 mM Tris–HCl, pH 8.0, containing 20% sucrose at room temperature. EDTA iron (III) salt (pH 7.5) and lysozyme were added to achieve final concentrations of 10 mM and 1 mg ml^{-1}, respectively, and incubated at 21 °C for 60 min. The spheroplasts were centrifuged at 16,000 g for 30 min at 4 °C and resuspended in 20 ml of 0.1 M phosphate buffer pH 7.5, which contained 20% sucrose. DNase and MgSO$_4$ were added to achieve final concentrations of 2 mg ml^{-1} and 20 mM, respectively. The spheroplast mixture was incubated at 37 °C for 1 h and broken by ultrasonication (15 min, pulsation at 10 s/10 s on–off) on ice. The cell debris was removed by centrifugation at 800 g for 10 min at 4 °C. The lysate was centrifuged at 75,000 g for 30 min at 4 °C (Beckmann Optima MAX Tabletop Ultracentrifuge) to obtain a crude inner membrane. Membranes were resuspended at 10 mg wet weight per ml into 50 mM phosphate buffer (pH 7.5) which contained 5 mM magnesium sulfate. Membrane preparations were stored at −80 °C until further use.

NADH-quinone oxidoreductase activity assay

Briefly, the bacterial inner membrane (1 mg ml^{-1}) was resuspended in 50 mM phosphate buffer (pH 7.5) containing 5 mM MgSO$_4$ and ubiquinone-1, and potassium cyanide was added to achieve final concentrations of 200 µM and 5 mM, respectively. BSS was added as desired, and the reaction mixture was incubated for 2 h at 37 °C. The reaction was initiated by adding 200 µM NADH immediately before each experiment. The NADH oxidase activity was measured by the decrease in absorbance at 340 nm using a spectrophotometer (Varioskan Flash; Thermo Scientific) for 2 h. For in vivo test, the reaction was started without the treatment of BSS. The membrane treated at 90 °C for 10 min was used as a negative control. All the tests were performed in triplicate.

PMF assay

The prodye BCECF-AM was used. This pro-dye is able to cross the bacterial membranes where it is hydrolysed by non-specific esterases to give a pH-sensitive dye, the fluorescence of which decreases as cytoplasmic pH decreases. Briefly, early growth logarithmic phase (OD$_{600}$ = 0.2–0.3) cultures were exposed to 25 µM BCECF-AM (Thermo) for 30 min at 37 °C. Loaded cells were washed three times with 0.9% NaCl and resuspended in a fresh CAMHB medium. Next, the cells were

incubated with the indicated concentration of BSS or carbonyl cyanide 3-chlorophenylhydrazone (CCCP) (40 µg ml^{-1}), a known proton uncoupler, as a positive control for 30 min at 37 °C. The fluorescence signal was monitored at excitation/emission of 500/522 nm by a spectrophotometer (Varioskan Flash; Thermo Scientific). The data shown are representative of results from six technical replicates.

Membrane potential assay

The bacteria were cultured at 37 °C in LB medium to an OD$_{600}$ of 1. The bacteria were diluted to 10^6 c.f.u. ml^{-1} in PBS. To each 1.5 ml of the bacterial suspension, 20 mM DiOC2(3) was added to achieve a final concentration of 15 µM and incubated for 1 h at 37 °C in the dark, followed by flow cytometry analysis (Accuri C6; BD). DiOC2(3) was excited at 484 nm, and the emissions at 530 nm (green fluorescence) and 610 nm (red fluorescence) were measured. All experiments were performed in triplicate. The green fluorescence is relatively independent of membrane potential and mainly reflects particle sizes, while the red fluorescence is highly dependent on membrane potential. Membrane potential was indicated by the red/green ratio. Gating strategy is shown in Supplementary Fig. 8.

Sdh assay

Sdh activity was measured by a Sdh assay kit (Abcom, ab228560). In this assay, Sdh converts succinate to fumarate and transfers the electron to an artificial electron acceptor (Probe), which changes the colour from blue to a colourless product. Briefly, the bacterial inner membrane (1 mg ml^{-1}) was resuspended in 50 mM phosphate buffer (pH 7.5) and treated with the indicated concentrations of BSS for 2 h at 37 °C. About 50 µl sample was mixed with 50 µl of Sdh reaction mix into 96 wells plate and measured absorbance (600 nm) at 25 °C in kinetic mode by a spectrophotometer (Varioskan Flash; Thermo Scientific). The activity of Sdh is evaluated based on the rate of decrease in relative absorbance values.

Aconitase enzyme activity assay

The aconitase activity was measured by an aconitase enzyme activity microplate assay kit (Abcom, ab109712). In this assay, aconitase catalyses an equilibrium between citrate, cis-aconitate and iso-citrate. These reactions are monitored by measuring the increase in absorbance at 240 nm associated with the formation of the cis-aconitate. Therefore, the rate of cis-aconitate production is proportional to aconitase activity. Briefly, the bacteria were cultured at 37 °C in CAMHB medium to early growth logarithmic phase (OD$_{600}$ = 0.2–0.3). Subsequently, the bacteria were treated with the indicated concentration of BSS at 37 °C for 2 h. The bacteria were collected by centrifugation and lysed in PBS by sonication. The protein concentrations were quantified by a BCA assay kit. About 50 µl sample (1 mg ml^{-1}) was mixed with 200 µl of reaction mix into a 96-well plate, and absorbance was measured (240 nm) at 25 °C in kinetic mode by a spectrophotometer (Varioskan Flash; Thermo Scientific). To analyse the data, two time points between which the rates are linearly increasing for all samples were picked. The aconitase activity was evaluated by calculating the average reaction rate (Rate = (Absorbance 1 − Absorbance 2)/time (min).

Bacterial ATP level assay

Bacterial intracellular ATP levels were determined using a BacTiter-GloTM Microbial Cell Viability Assay (Promega) kit. The bacteria were cultured at 37 °C in CAMHB medium to early growth logarithmic phase (OD$_{600}$ = 0.2–0.3). Subsequently, the bacteria were treated with the indicated concentration of BSS, ERV or their combinations at 37 °C for 1 h. About 50 µl BacTiter-GloTM reagent was mixed with 50 µl cell culture and incubated for 5 min at room temperature. Luminescence was measured with a luminometer (Tecan). At the same time, the number of viable bacteria was counted by dilution and plating. The ATP concentration was calculated using a standard curve made with a commercial ATP

solution. Relative ATP levels were calculated based on bacteria counts. All the tests were performed in triplicate.

EtBr efflux assay

The bacteria were cultured in a CAMHB medium at 37 °C to an OD_{600} of 1. The cells were washed with 10 mM HEPES) buffer and adjusted to $OD_{600} = 0.5$. EtBr was added at a final concentration of 5 µM, and cells were incubated for 30 min at 37 °C. The cells were collected by centrifugation and resuspended in a fresh CAMHB medium containing the indicated concentration of BSS or 40 mg l^{-1} CCCP as a control. The fluorescence signal was monitored at an excitation/emission wavelength of 525/600 nm every 5 min for 120 min at 37 °C with a luminometer (Varioskan Flash; Thermo Scientific). The data shown are representative of results from three technical replicates.

Tetracycline accumulation assays

Tetracyclines have strong ultraviolet absorption and fluorescence properties in the near-visible region. Therefore, we detected the accumulation of tetracycline by fluorescence. PAO1 was grown in CAMHB to an OD_{600} of 1 and then incubated with 50 mg l^{-1} of ERV in the presence or absence of different concentrations of BSS for 15 min. The bacteria were collected by centrifugation and washed three times with PBS. The bacterial cells were lysed in PBS by sonication. The fluorescence of ERV was measured at an excitation/emission wavelength of 400/520 nm with a luminometer (Varioskan Flash; Thermo Scientific). Total bacterial protein concentrations were quantified by BCA assays.

Antibiotics uptake assay

To quantify the uptake of other antibiotics (azithromycin, chloramphenicol, ofloxacin), bacteria were grown in CAMHB to an OD_{600} of 1 and then incubated with antibiotic (8 mg l^{-1} for azithromycin and chloramphenicol, 0.5 mg l^{-1} for ofloxacin) in the presence of different concentrations of BSS for 1 h. The bacteria were collected by centrifugation and washed three times with PBS. The bacterial cells were lysed in PBS by sonication. The cellular antibiotic levels were measured using a specific antibiotic ELISA Kit. Total bacterial protein concentrations were quantified by BCA assay.

RNA isolation, RT-qPCR and transcriptome analysis

Overnight cultured PAO1 cells were diluted 1:100 into CAMHB and incubated at 37 °C to an OD_{600} of 1. The cells were treated with 16 µM BSS for 30 min. The cells were collected and resuspended in 1 ml of TRIzol reagent (Life Technologies). Total bacterial RNA was extracted by chloroform-isopropanol precipitation. The residual DNA was digested with RNase-free recombinant DNase I (Roche), the RNA was dissolved in RNase-free water, and complementary DNA was synthesized using random primers and reverse transcriptase (Invitrogen). SYBR II Green supermix (BioRed) was used for qPCR, and the ribosomal gene *rpsL* was used as an internal reference control. All the tests were performed in triplicate. The Zymo-Seq RiboFree Total RNA Library Kit (Zymo Research) was used to prepare the library preps for Illumina sequencing using 800 ng of the extracted total RNA. Samples were sequenced on the Illumina NexSeq 500 to generate 75 bases single-end reads (75SE) with an average read depth of 12 M reads per sample. The quality of the resulting fastq reads was checked using FastQC v0.11.9 (Babraham Bioinformatics) and mapped on the reference genome using Bowtie2 v2.4.2 using default settings. The resulting SAM files were converted to BAM using SAMtools 1.11, and feature Counts 2.0.1 was used to get the gene counts. The T-REx webserver was used to perform statistical analyses and determine differential gene expressions.

Resistance development analysis

The evolution of ERV and ofloxacin resistance in vitro was characterized by a standard sequential passaging technique. *P. aeruginosa* PAO1 cells were grown in CAMHB medium to exponential phase at 37 °C. The MICs of ERV in the presence or absence of 16 µM BSS were determined by standard broth microdilution in 96-well plates and monitored for 25 days. The plate was incubated for 18 h under static conditions at 37 °C. The sub-MIC (0.25 × MIC) bacterial suspension from the ERV or BSS + ERV combination was diluted in CAMHB to a final concentration of 10^6 c.f.u. ml^{-1} to prepare the inoculum for the next-day MIC experiment. Experiments were performed with three biological replicates.

Biofilm killing assay

Overnight cultured PAO1 cells were diluted 1:100 into CAMHB and incubated at 37 °C to an OD_{600} of 1. The bacterial suspension was standardized to an $OD_{600} = 0.025$ in fresh CAMHB. About 1 ml of bacterial suspension was added into a glass tube and incubated at 37 °C for 24 h to form the biofilm. Due to the strong antibiotic resistance nature of biofilms, 1×, 1/2×, 1/4× and 1/8× MIC of antibiotics combined with 32 µM BSS was used to kill the established biofilm for 24 h. Finally, the biofilm was washed three times with sterile PBS and treated with 2 ml fresh CAMHB containing the indicated concentration of antibiotics or BSS or the combination at 37 °C for 24 h. The tube was washed three times with sterile PBS, the biofilm was dispersed by ultrasound, and the numbers of bacteria were determined by plating. The experiment was performed in triplicate.

Antimicrobial activity in blood

Human blood of healthy individuals was obtained from Sanquin with approval for research use (certified Dutch organization responsible for meeting the need in healthcare for blood and blood products; the reference number assigned was NVT0523.01) and was infected with 5 × 10^7 c.f.u. ml^{-1} of PAO1. The blood was distributed at 0.5 ml in 2 ml Eppendorf tubes and treated with the indicated concentration of antibiotics or bismuth compounds or their combination at 37 °C. At 4 h post infection, the samples were decimal serially diluted in PBS. Drops of 10 µl of each dilution on LB agar were used to track the number of remaining viable bacteria. At 24 h post infection, the samples were photographed to track the development of infection. The experiment was performed in triplicate.

Mammalian cell toxicity

Cytotoxicity was determined using a Cell Proliferation Kit II (XTT) (Roche). The human lung epithelial cells (A549) and embryonic kidney cells (HEK293T) were cultured in Dulbecco's modified Eagle medium with 2% (vol/vol) heat-inactivated fetal bovine serum at 37 °C with 5% CO_2. A total of 2 × 10^4 cells were seeded into each well of a 96-well plate and cultured overnight. The drug was added to each well, resulting in the indicated final concentrations and incubated at 37 °C with 5% CO_2 for 48 h. After the addition of 50 µl XTT working solution to each well, the plate was incubated at 37 °C with 5% CO_2 for 4 h. The absorbance at 495 nm was measured using a luminometer (Varioskan Flash; Thermo Scientific). The cell viability was calculated using untreated cells as a control.

Haemolysis assay on human red blood cells

For erythrocyte isolation, blood was centrifuged at 1,000 *g* at 4 °C for 10 min, and the supernatant was removed. After that, the cells were washed three times with 0.9% NaCl solution in the same conditions and finally resuspended in the same buffer. In a 96-well plate, 160 µl of 10-fold diluted red cells were added, and the drugs were added in a volume of 40 µl of 0.9% NaCl to give rise to a final concentration of the drugs ranging from 8 to 256 µM. Triton X-100 at 1% was used as a positive lysis control. The plate was incubated at 37 °C for 1 h. After that, samples were centrifuged (1,000 *g* for 10 min at 4 °C) to remove the intact erythrocytes, and the supernatant was transferred to a new 96-well plate. The absorbance of released haemoglobin was measured at OD_{540}, and the percentage of haemolysis was calculated.

Bismuth biodistribution in mice

All animal experiments were approved by and performed in accordance with the guidelines approved by the Committee on the Use of Live Animals in Teaching and Research (CULATR), the University of Hong Kong and the 'Guide for the Care and Use of Laboratory Animals' as promulgated by the National Institute of Health, Animal Research: Reporting of In Vivo Experiments guidelines and the protocols approved by the Ethics Committee of Laboratory Animals of the University of Granada. All the experiments were performed according to the standard operating procedures of the biosafety level 2 animal facilities (reference number CULATR 5079-19 and 26072017). For the toxicity test, two lines of mice were tested BALB/c and C57Bl/6. For the acute toxicity test, the mice were randomly divided into 3 study groups (n = 4) and anaesthetized with an intraperitoneal injection of ketamine (100 mg kg^{-1}) and xylazine (10 mg kg^{-1}), followed by inoculation with 20 µl CBS solution, resulting in a dosage of 100 mg kg^{-1} or 200 mg kg^{-1}. The appearance, behaviour and response to stimuli of the mice were observed after administration to evaluate possible acute toxicity, and the mice's body weights were recorded for 7 days. A similar approach was used in the case of C57Bl/6. Adults (8–10 weeks old, male) were randomized and divided into 3 study groups (n = 4). Mice were anaesthetized as before, and then 100 mg kg^{-1} CBS was applied intranasally in a final volume of 50 µl in PBS, each mice receiving a unique dose of the compound or one dose per day for 3 consecutive days. After 24 or 72 h from the last administration, mice were killed by cervical dislocation. A control group (control n = 4) was included for reference, which was given the vehicle. Then, the mouse body weights were recorded. Kidneys, lungs and livers were removed aseptically, and tissues were weighed, frozen in liquid nitrogen and stored at −80 °C.

To determine the organs-associated concentration of bismuth ions, the 6- to 8-week-old female BALB/c mice were randomly divided into 3 study groups (n = 4) and anaesthetized with an intraperitoneal injection of ketamine (100 mg kg^{-1}) and xylazine (10 mg kg^{-1}), followed by inoculation with 20 µl CBS solution, resulting in a dosage of 100 mg kg^{-1}. The mice of each group were euthanized by intraperitoneal injection of 100 mg kg^{-1} pentobarbitone at 4, 8 and 24 h post treatment. The organs were isolated and weighed, then subjected to homogenization in 1 ml PBS. About 100 µl of the homogenized tissues were added into 900 µl 68% HNO$_3$ and incubated at 65 °C overnight. The dissolved samples were diluted to the appropriate concentrations for the quantification of metals by ICP-MS (Agilent 7500a, Agilent Technologies).

Mouse acute pneumonia model

In all mice studies, 6- to 8-week-old female BALB/c mice were used. Briefly, overnight cultured PAO1 cells were diluted 1:100 in fresh LB and incubated at 37 °C to an OD$_{600}$ of 1. The collected bacterial cells were washed once with PBS. The bacterial concentration was adjusted to 3×10^9 c.f.u. ml^{-1} in PBS. Each female BALB/c mouse was anaesthetized with an intraperitoneal injection of ketamine (100 mg kg^{-1}) and xylazine (10 mg kg^{-1}), followed by inoculation with 20 µl of the bacterial suspension, resulting in 6×10^7 c.f.u. per mouse. The mice were administered half an hour post infection intranasally with a 20 µl aliquot of PBS, monotherapy of antibiotic or CBS or their combinatory therapy (n = 8). Body weights and mouse survival were monitored till the end point of the experiment.

For lung colonization and histological studies, a sub-lethal dose of bacteria (4×10^7 c.f.u. per mouse) was used. The mice were euthanized by intraperitoneal injection of 100 mg kg^{-1} pentobarbitone 24 h post treatment. Lungs were isolated and subjected to homogenization. The bacterial load in each lung was determined by plating (n = 8). For histological studies, lung samples were obtained from mice and stored in 10% formalin for 48 h and rinsed with 70% ethanol (n = 3). Tissues were embedded in paraffin, thin-sectioned, stained with haematoxylin and eosin and examined by microscopy.

Reporting summary

Further information on research design is available in the Nature Portfolio Reporting Summary linked to this article.

Data availability

The transcriptome (RNA sequencing) data that support the findings of this study have been deposited in the National Center for Biotechnology Information Gene Expression Omnibus (GEO) with the accession code GSE223542. Genome sequencing data for the antibiotics resistant isolates are available in the National Center for Biotechnology Information Sequence Read Archive under the accession number PRJNA1089519. Source data are provided with this paper.

References

1. Piddock, L. J. V. Reflecting on the final report of the O'Neill Review on Antimicrobial Resistance. *Lancet Infect. Dis.* **16**, 767–768 (2016).
2. Prestinaci, F., Pezzotti, P. & Pantosti, A. Antimicrobial resistance: a global multifaceted phenomenon. *Pathog. Glob. Health* **109**, 309–318 (2015).
3. Marston, H. D., Dixon, D. M., Knisely, J. M., Palmore, T. N. & Fauci, A. S. Antimicrobial resistance. *JAMA* **316**, 1193–1204 (2016).
4. Flamm, R. K. et al. Factors associated with relative rates of antibiotic resistance in *Pseudomonas aeruginosa* isolates tested in clinical laboratories in the United States from 1999 to 2002. *Antimicrob. Agents Chemother.* **48**, 2431–2436 (2004).
5. Qin, S. et al. *Pseudomonas aeruginosa*: pathogenesis, virulence factors, antibiotic resistance, interaction with host, technology advances and emerging therapeutics. *Signal Transduct. Target. Ther.* **7**, 199 (2022).
6. Lister, P. D., Wolter, D. J. & Hanson, N. D. Antibacterial-resistant *Pseudomonas aeruginosa*: clinical impact and complex regulation of chromosomally encoded resistance mechanisms. *Clin. Microbiol. Rev.* **22**, 582–610 (2009).
7. Costerton, J. W., Lewandowski, Z., Caldwell, D. E., Korber, D. R. & Lappin-Scott, H. M. Microbial biofilms. *Annu. Rev. Microbiol.* **49**, 711–745 (1995).
8. Theuretzbacher, U., Outterson, K., Engel, A. & Karlén, A. The global preclinical antibacterial pipeline. *Nat. Rev. Microbiol.* **18**, 275–285 (2020).
9. Kupferschmidt, K. Resistance fighters. *Science* **352**, 758–761 (2016).
10. Theuretzbacher, U. et al. Critical analysis of antibacterial agents in clinical development. *Nat. Rev. Microbiol.* **18**, 286–298 (2020).
11. Sun, H. et al. Resensitizing carbapenem- and colistin-resistant bacteria to antibiotics using auranofin. *Nat. Commun.* **11**, 5263 (2020).
12. Wang, C. et al. Metallo-sideromycin as a dual functional complex for combating antimicrobial resistance. *Nat. Commun.* **14**, 5311 (2023).
13. Tyers, M. & Wright, G. D. Drug combinations: a strategy to extend the life of antibiotics in the 21st century. *Nat. Rev. Microbiol.* **17**, 141–155 (2019).
14. Bollenbach, T. Antimicrobial interactions: mechanisms and implications for drug discovery and resistance evolution. *Curr. Opin. Microbiol.* **27**, 1–9 (2015).
15. Kanatzidis, M., Sun, H. & Dehnen, S. Bismuth-the magic element. *Inorg. Chem.* **59**, 3341–3343 (2020).
16. Griffith, D. M., Li, H., Werrett, M. V., Andrews, P. C. & Sun, H. Medicinal chemistry and biomedical applications of bismuth-based compounds and nanoparticles. *Chem. Soc. Rev.* **50**, 12037–12069 (2021).
17. Li, H. & Sun, H. Recent advances in bioinorganic chemistry of bismuth. *Curr. Opin. Chem. Biol.* **16**, 74–83 (2012).

18. Malfertheiner, P. Infection: bismuth improves PPI-based triple therapy for *H. pylori* eradication. *Nat. Rev. Gastroenterol. Hepatol.* **7**, 538–539 (2010).

19. Alkim, H., Koksal, A. R., Boga, S., Sen, I. & Alkim, C. Role of bismuth in the eradication of *Helicobacter pylori*. *Am. J. Ther.* **24**, e751–e757 (2017).

20. Wang, R. et al. Bismuth antimicrobial drugs serve as broad-spectrum metallo-β-lactamase inhibitors. *Nat. Commun.* **9**, 439 (2018).

21. Deng, T. et al. Bismuth drugs reverse Tet(X)-conferred tigecycline resistance in gram-negative bacteria. *Microbiol. Spectr.* **10**, e0157821 (2022).

22. Fiorini, G. et al. Rescue therapy with bismuth quadruple regimen in patients with *Helicobacter pylori*-resistant strains. *Helicobacter* **22**, e12448 (2017).

23. Tacconelli, E. et al. Discovery, research, and development of new antibiotics: the WHO priority list of antibiotic-resistant bacteria and tuberculosis. *Lancet Infect. Dis.* **18**, 318–327 (2018).

24. Imamura, Y. et al. Azithromycin exhibits bactericidal effects on *Pseudomonas aeruginosa* through interaction with the outer membrane. *Antimicrob. Agents Chemother.* **49**, 1377–1380 (2005).

25. Murdoch, C. C. & Skaar, E. P. Nutritional immunity: the battle for nutrient metals at the host–pathogen interface. *Nat. Rev. Microbiol.* **20**, 657–670 (2022).

26. Andrews, S. C., Robinson, A. K. & Rodríguez-Quiñones, F. Bacterial iron homeostasis. *FEMS Microbiol. Rev.* **27**, 215–237 (2003).

27. Xia, W., Li, H., Yang, X., Wong, K. B. & Sun, H. Metallo-GTPase HypB from *Helicobacter pylori* and its interaction with nickel chaperone protein HypA. *J. Biol. Chem.* **287**, 6753–6763 (2012).

28. Braud, A., Hannauer, M., Mislin, G. L. & Schalk, I. J. The *Pseudomonas aeruginosa* pyochelin-iron uptake pathway and its metal specificity. *J. Bacteriol.* **191**, 3517–3525 (2009).

29. Lamont, I. L., Beare, P. A., Ochsner, U., Vasil, A. I. & Vasil, M. L. Siderophore-mediated signaling regulates virulence factor production in *Pseudomonas aeruginosa*. *Proc. Natl Acad. Sci. USA* **99**, 7072–7077 (2002).

30. He, X., Liao, X., Li, H., Xia, W. & Sun, H. Bismuth-induced inactivation of ferric uptake regulator from *Helicobacter pylori*. *Inorg. Chem.* **56**, 15041–15048 (2017).

31. Meylan, S. et al. Carbon sources tune antibiotic susceptibility in *Pseudomonas aeruginosa* via tricarboxylic acid cycle control. *Cell Chem. Biol.* **24**, 195–206 (2017).

32. Baradaran, R., Berrisford, J. M., Minhas, G. S. & Sazanov, L. A. Crystal structure of the entire respiratory complex I. *Nature* **494**, 443–448 (2013).

33. Poulsen, B. E. et al. Defining the core essential genome of *Pseudomonas aeruginosa*. *Proc. Natl Acad. Sci. USA* **116**, 10072–10080 (2019).

34. Wang, Y. et al. Integrative approach for the analysis of the proteome-wide response to bismuth drugs in *Helicobacter pylori*. *Chem. Sci.* **8**, 4626–4633 (2017).

35. Ito, A. et al. Siderophore cephalosporin cefiderocol utilizes ferric iron transporter systems for antibacterial activity against *Pseudomonas aeruginosa*. *Antimicrob. Agents Chemother.* **60**, 7396–7401 (2016).

36. Cochrane, S. A. et al. Antimicrobial lipopeptide tridecaptin A1 selectively binds to Gram-negative lipid II. *Proc. Natl Acad. Sci. USA* **113**, 11561–11566 (2016).

37. Wen, Z. et al. Mechanism of eravacycline resistance in clinical *Enterococcus faecalis* isolates from China. *Front. Microbiol.* **11**, 916 (2020).

38. Lebeaux, D., Ghigo, J. M. & Beloin, C. Biofilm-related infections: bridging the gap between clinical management and fundamental aspects of recalcitrance toward antibiotics. *Microbiol. Mol. Biol. Rev.* **78**, 510–543 (2014).

39. Hong, Y., Lai, Y. T., Chan, G. C. & Sun, H. Glutathione and multidrug resistance protein transporter mediate a self-propelled disposal of bismuth in human cells. *Proc. Natl Acad. Sci. USA* **112**, 3211–3216 (2015).

40. Meyer, J. M., Neely, A., Stintzi, A., Georges, C. & Holder, I. A. Pyoverdin is essential for virulence of *Pseudomonas aeruginosa*. *Infect. Immun.* **64**, 518–523 (1996).

41. Goss, C. H. et al. Gallium disrupts bacterial iron metabolism and has therapeutic effects in mice and humans with lung infections. *Sci. Transl. Med.* **10**, eaat7520 (2018).

42. Zhang, Q. et al. Re-sensitization of mcr carrying multidrug resistant bacteria to colistin by silver. *Proc. Natl Acad. Sci. USA* **119**, e2119417119 (2022).

43. Wang, H. et al. Multi-target mode of action of silver against *Staphylococcus aureus* endows it with capability to combat antibiotic resistance. *Nat. Commun.* **12**, 3331 (2021).

44. Frei, A., Verderosa, A. D., Elliott, A. G., Zuegg, J. & Blaskovich, M. A. T. Metals to combat antimicrobial resistance. *Nat. Rev. Chem.* **7**, 202–224 (2023).

45. Schalk, I. J. & Cunrath, O. An overview of the biological metal uptake pathways in *Pseudomonas aeruginosa*. *Environ. Microbiol.* **18**, 3227–3246 (2016).

46. Palma, M., Worgall, S. & Quadri, L. E. Transcriptome analysis of the *Pseudomonas aeruginosa* response to iron. *Arch. Microbiol.* **180**, 374–379 (2003).

47. Kaneko, Y., Thoendel, M., Olakanmi, O., Britigan, B. E. & Singh, P. K. The transition metal gallium disrupts *Pseudomonas aeruginosa* iron metabolism and has antimicrobial and antibiofilm activity. *J. Clin. Invest.* **117**, 877–888 (2007).

48. Efremov, R. G. & Sazanov, L. A. Structure of the membrane domain of respiratory complex I. *Nature* **476**, 414–420 (2011).

49. Yuan, S. et al. Metallodrug ranitidine bismuth citrate suppresses SARS-CoV-2 replication and relieves virus-associated pneumonia in Syrian hamsters. *Nat. Microbiol.* **5**, 1439–1448 (2020).

50. Wang, R. et al. Orally administered bismuth drug together with N-acetyl cysteine as a broad-spectrum anti-coronavirus cocktail therapy. *Chem. Sci.* **13**, 2238–2248 (2022).

51. Tillman, L. A., Drake, F. M., Dixon, J. S. & Wood, J. R. Review article: safety of bismuth in the treatment of gastrointestinal diseases. *Aliment. Pharmacol. Ther.* **10**, 459–467 (1996).

Acknowledgements

Author contributions

O.P.K., H.S. and R.C. conceived and designed the project; Y.X., X.W., P.G., C.W. and R.C. conducted the experiments and data analyses. A.d.J. performed the transcriptome analysis. J.H.K.C. performed the collections of clinical *P. aeruginosa* isolates. M.J.R.-S., A.R.-N., P.D.-E, J.G. and F.G. performed the toxicity test in C57Bl/6 mice. Y.X., X.W. and P.G. performed the in vivo test in BALB/c mice. W.W., R.Y.-T.K. and H.L. provided the suggestions. Y.X., H.L., R.C., H.S. and O.P.K. prepared the paper with contributions from all other authors. All the authors approved the final paper.

Competing interests

O.P.K., Y.X. and R.C. are coinventors on a patent application associated with this work entitled 'synergistic composition against *Pseudomonas aeruginosa*', with reference number N2029436 (2021). O.P.K. is also cofounder and board member of the company Omnicin Therapeutics that is developing novel therapies against *P. aeruginosa*. The other authors declare no competing interests.

Additional information

Extended data is available for this paper at https://doi.org/10.1038/s41564-024-01807-6.

Supplementary information The online version contains supplementary material available at https://doi.org/10.1038/s41564-024-01807-6.

Correspondence and requests for materials should be addressed to Rubén Cebrián, Oscar P. Kuipers or Hongzhe Sun.

Peer review information *Nature Microbiology* thanks Kim Lewis and the other, anonymous, reviewer(s) for their contribution to the peer review of this work. Peer reviewer reports are available.

Reprints and permissions information is available at www.nature.com/reprints.

Publisher's note Springer Nature remains neutral with regard to jurisdictional claims in published maps and institutional affiliations.

Springer Nature or its licensor (e.g. a society or other partner) holds exclusive rights to this article under a publishing agreement with the author(s) or other rightsholder(s); author self-archiving of the accepted manuscript version of this article is solely governed by the terms of such publishing agreement and applicable law.

© The Author(s), under exclusive licence to Springer Nature Limited 2024

[1]Department of Chemistry, State Key Laboratory of Synthetic Chemistry, CAS-HKU Joint Laboratory of Metallomics on Health and Environment, The University of Hong Kong, Hong Kong, China. [2]Department of Molecular Genetics, Groningen Biomolecular Sciences and Biotechnology Institute, University of Groningen, Groningen, Netherlands. [3]State Key Laboratory of Medicinal Chemical Biology, Key Laboratory of Molecular Microbiology and Technology of the Ministry of Education, Department of Microbiology, College of Life Sciences, Nankai University, Tianjin, China. [4]Department of Microbiology, School of Clinical Medicine, Li Ka Shing Faculty of Medicine, The University of Hong Kong, Hong Kong, China. [5]Department of Microbiology, The University of Hong Kong and Queen Mary Hospital, Hong Kong, China. [6]Department of Digestive system, Instituto de Investigación Biosanitaria ibs. GRANADA, University Hospital Virgen de las Nieves, Granada, Spain. [7]Department of Pharmacology, Instituto de Investigación Biosanitaria ibs. GRANADA, Center for Biomedical Research (CIBM), University of Granada, Granada, Spain. [8]Biomedical Research Network Center, Liver and Digestive Diseases (CIBER-EHD), Granada, Spain. [9]Department of Clinical Microbiology, Instituto de Investigación Biosanitaria ibs. GRANADA, University Hospital San Cecilio, Granada, Spain. [10]Biomedicinal Research Network Center, Infectious Diseases (CIBER-INFEC), Granada, Spain. ✉e-mail: rcebrian@ugr.es; o.p.kuipers@rug.nl; hsun@hku.hk
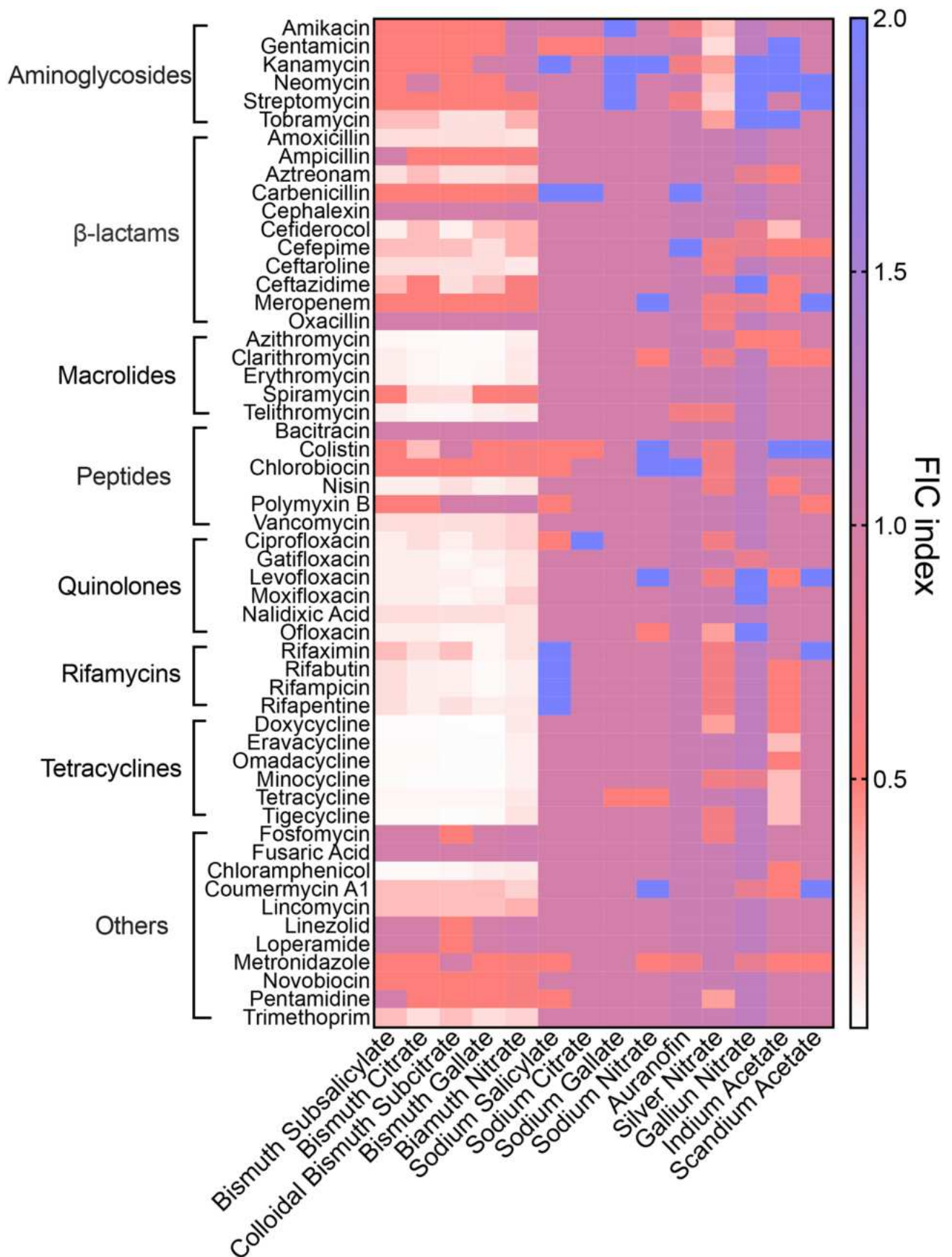
Extended Data Fig. 1 | Bismuth compounds show strong synergistic effects with multiple antibiotics against PAO1. The heat map of the FIC indices showing the synergistic effects of 55 antimicrobial agents with five different bismuth drugs against PAO1, while such synergistic effects were not observable for their sodium counterpart salts and other five metal-based compounds.
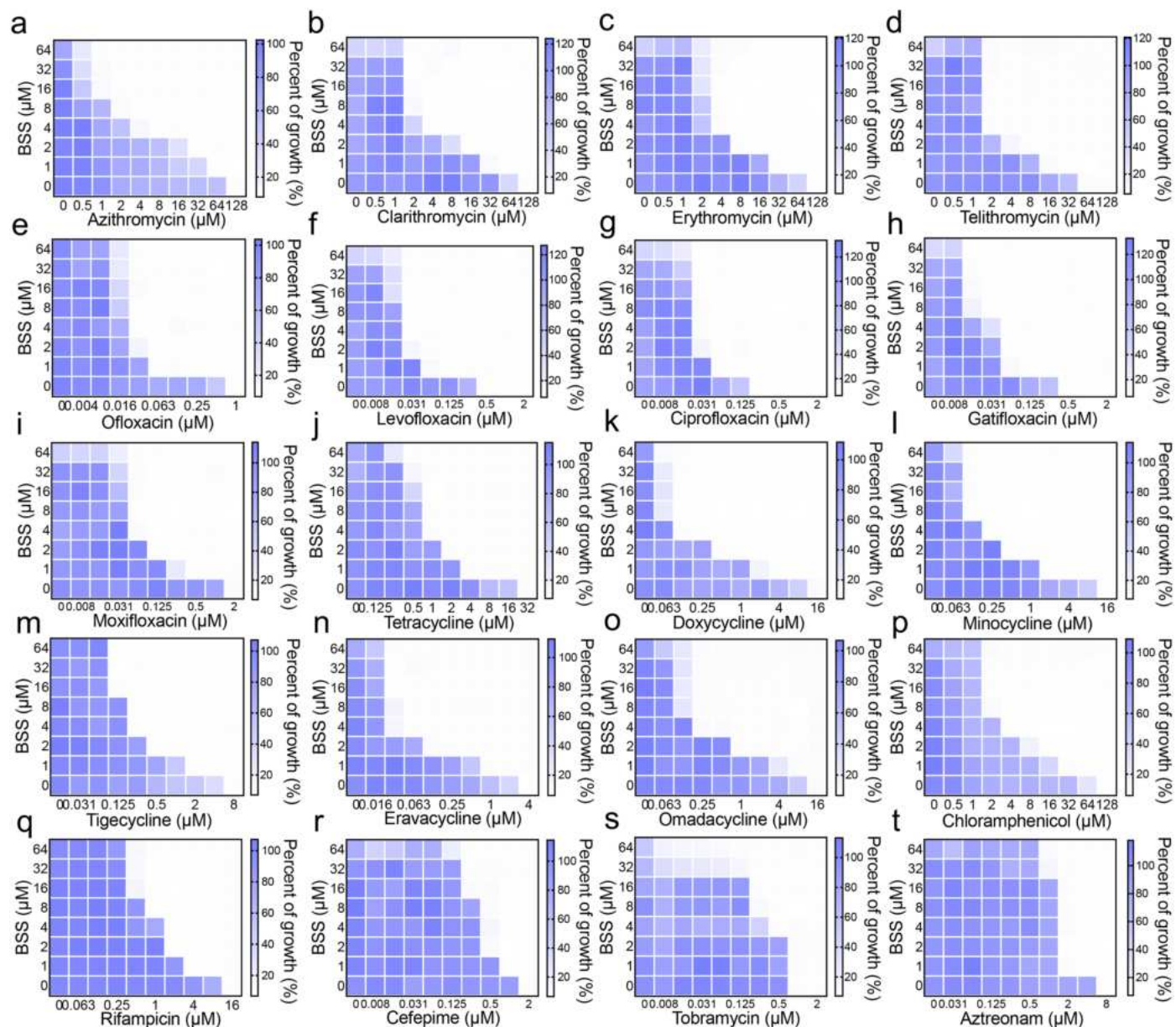
Extended Data Fig. 2 | Bismuth enhances the antimicrobial activity of multiple antibiotics against *P. aeruginosa* at a low concentration. Representative heat plots of microdilution checkerboard assay for the combination of antibiotics (azithromycin (**a**), clarithromycin (**b**), erythromycin (**c**), telithromycin (**d**), ofloxacin (**e**), levofloxacin (**f**), ciprofloxacin (**g**), gatifloxacin (**h**), moxifloxacin (**i**), tetracycline (**j**), doxycycline (**k**), minocycline (**l**), tigecycline (**m**), eravacycline (**n**), omadacycline (**o**), chloramphenicol (**p**), rifampicin (**q**), cefepime (**r**), tobramycin (**s**) and aztreonam (**t**)) with BSS against PAO1.
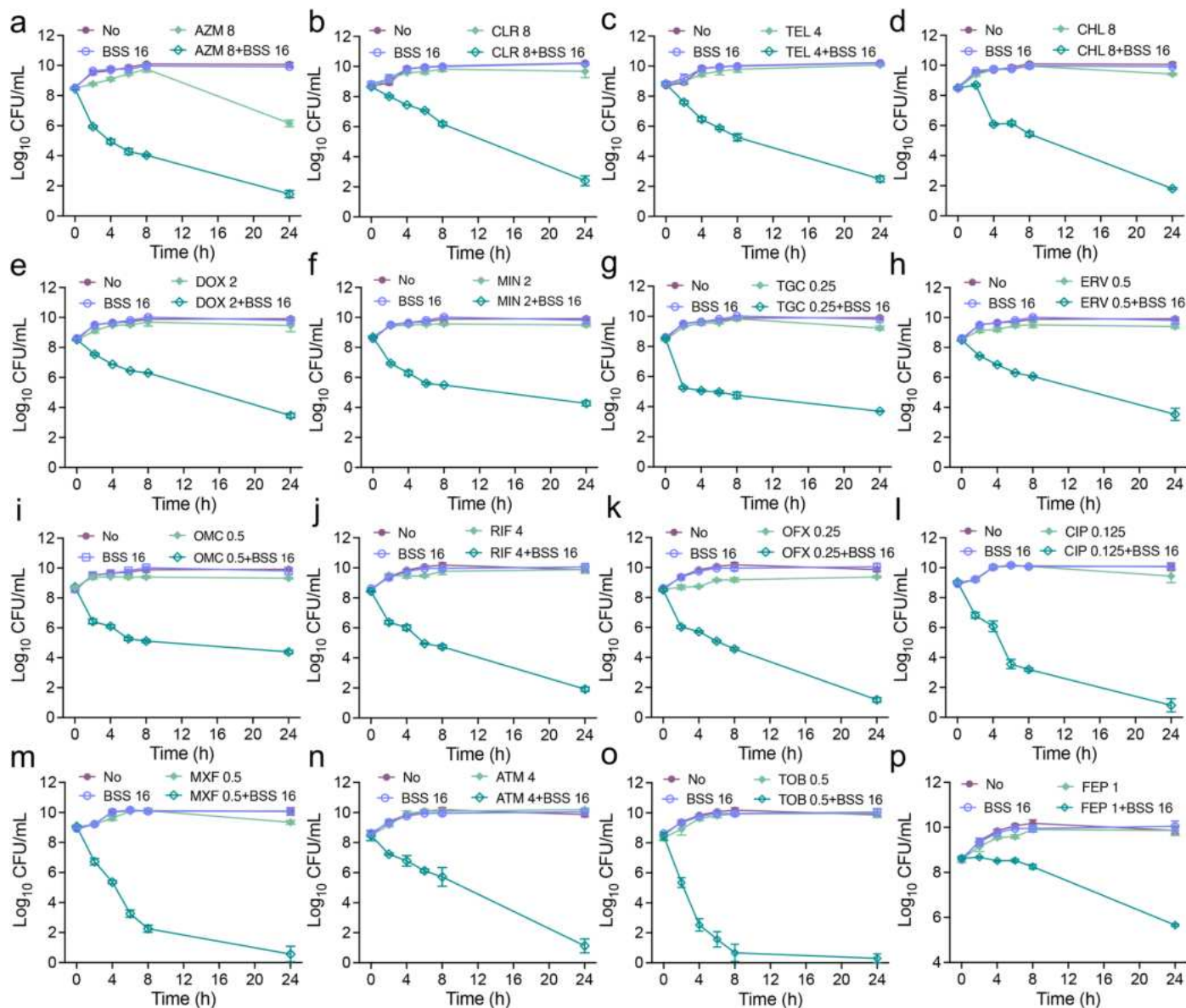
Extended Data Fig. 3 | Time-killing curves showed the synergistic effects of BSS and antibiotics against PAO1. Time-killing curves for antibiotics (azithromycin (AZM, **a**), clarithromycin (CLR, **b**), telithromycin (TEL, **c**), chloramphenicol (CHL, **d**), doxycycline (DOX, **e**), minocycline (MIN, **f**), tigecycline (TGC, **g**), eravacycline (ERV, **h**), omadacycline (OMC, **i**), rifampicin (RIF, **j**), ofloxacin (OFX, **k**), ciprofloxacin (CIP, **l**), moxifloxacin (MXF, **m**), aztreonam (ATM, **n**), tobramycin (TOB, **o**), cefepime (FEP, **p**)) and BSS monotherapy and their combination therapy against PAO1 during 24 h incubation at the indicated concentration (μM). Error bars represent mean ± SD for three biological replicates.
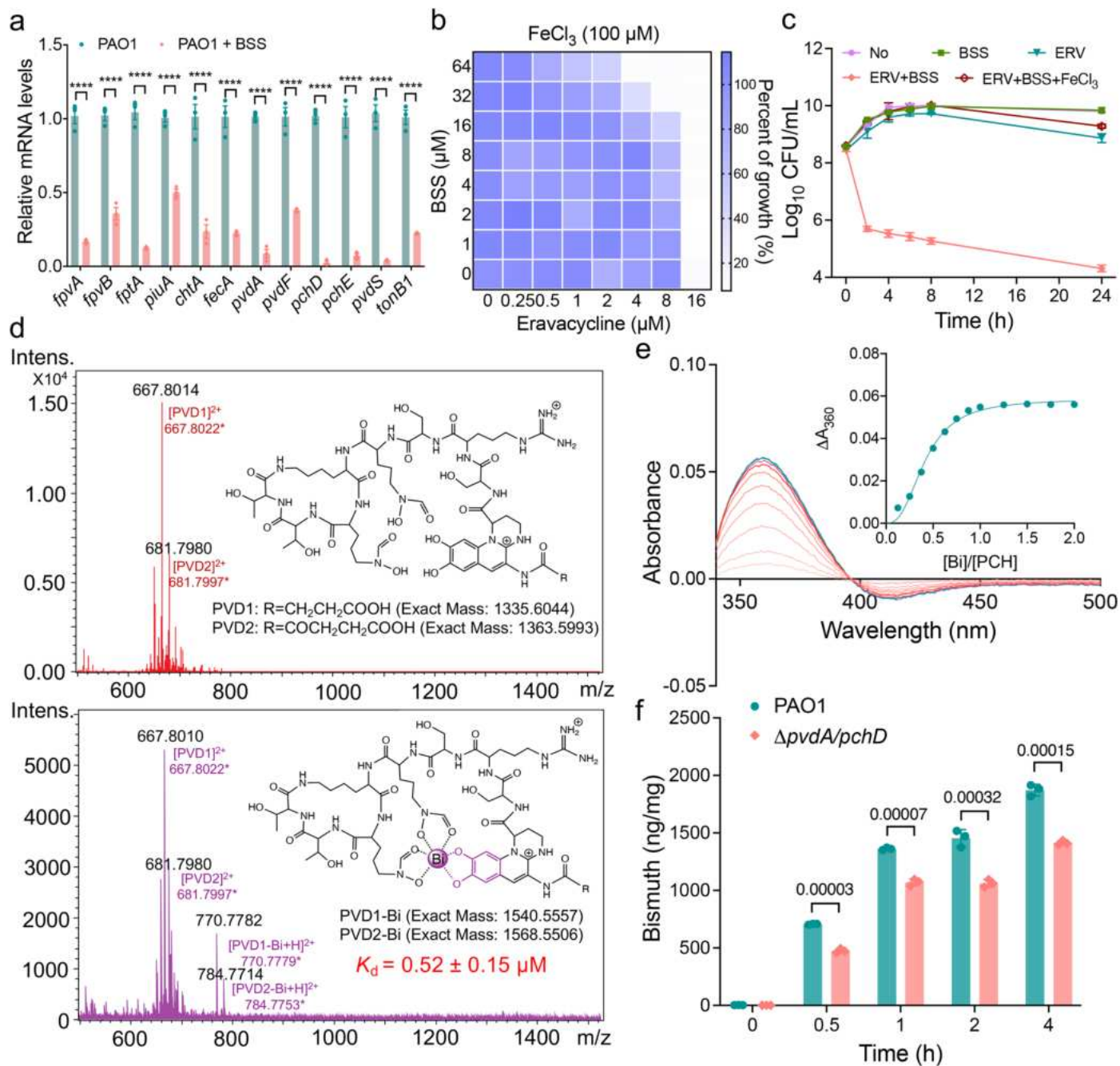
Extended Data Fig. 4 | Bismuth disrupts the iron homeostasis of
***P. aeruginosa.* a**, The RT-qPCR confirmed the downregulation of iron uptake-
related genes under the treatment of BSS. **b**, The heat map shows the lack of
synergy of bismuth with eravacycline in the presence of 100 μM FeCl₃. **c**, Time
killing curves for ERV (0.5 μM) and BSS (16 μM) monotherapy or combination
therapy against PAO1 in the absence or presence of 50 μM FeCl₃. **d**, The mass
spectra of PVD and bismuth-bound PVD (PVD-Bi). The peak at *m/z* of 667.8014
and 681.7980, assignable as PVD1 (Cald.667.8022) and PVD2 (Cald. 681.7997),
and two different side chains of PVD are noted. The appearance of two new
peaks after incubation of PVD with Bi(III) (as Bi(NO₃)₃) at *m/z* of 770.7782 and
784.7714 assignable to PVD1-Bi (Cald. 770.7779) and PVD2-Bi (Cald. 784.7753)

indicated binding of Bi to PVD at a 1:1 ratio. **e**, Different UV-vis spectra of PCH
upon addition of 0.125–2 molar equivalents of Bi(NTA). The inset shows the
changes in absorbance at 360 nm. **f**, The intracellular bismuth concentrations of
PAO1 and *pvdA/pchD* deletion strain under the treatment of 16 μM BSS. For Fig. a,
error bars represent mean ± SEM for three biological replicates. ****. P < 0.0001;
by two-sided unpaired t-test, 95% confidence interval. *fpvA*: P = 0.000048, *fpvB*:
P = 0.000146, *fptA*: P = 0.000033, *piuA*: P = 0.000109, *chtA*: P = 0.000542, *fecA*:
P = 0.000202, *pvdA*: P = 0.000008, *pvdF*: P = 0.000245, *pchD*: P = 0.000003,
pchE: P = 0.000118, *pvdS*: P = 0.000043, *tonB1*:P = 0.000052. For Fig. c and f,
error bars represent mean ± SEM for three biological replicates. For Fig. f, P values
were determined using two-sided unpaired t-test, 95% confidence interval.
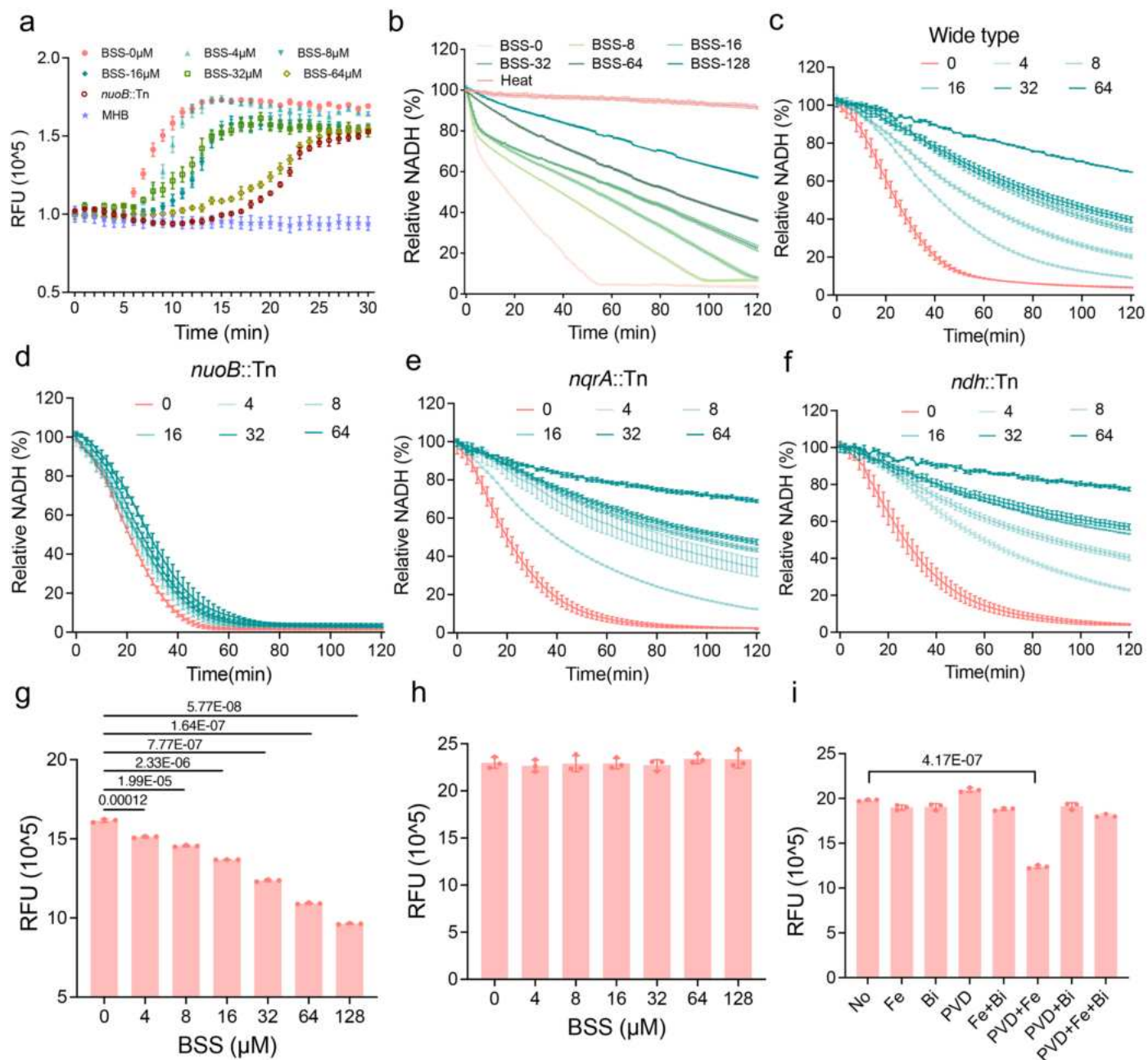
**Extended Data Fig. 5 | Bismuth impairs the activity of the electron transport chain (ETC) and promotes intracellular antibiotic accumulation in *P. aeruginosa*. a**, Time-dependent oxygen consumption rate was quantified by a fluorescence probe in the presence of indicated concentrations of BSS. The decrease in the oxygen consumption rate by BSS suggests the inhabitation of ETC activities. **b**, BSS inhibits the activity of NADH dehydrogenase *in vivo*. The bacteria were treated with different concentrations of BSS (μM) for 2 hours, then the inner membrane was collected and membrane-bound NADH-quinone oxidoreductase activity was measured. **c–f**, BSS dose-dependent inhibition on the activity of NADH dehydrogenase from different gene mutant strains. The bacterial inner membrane was collected and treated with different concentrations of BSS (μM) for 2 hours, then the membrane-bound NADH-quinone oxidoreductase activity was measured. **g**, The fluorescence of calcein inside of *P. aeruginosa* under the treatment of indicated concentrations of BSS.

h, The fluorescence of calcein inside of *P. aeruginosa* under the treatment of BSS in M9 medium without iron. The calcein-AM is not able to be quenched by bismuth or the change of metabolism and pH **i**, The fluorescence of calcein inside of *P. aeruginosa* under the treatment of different combinations of BSS (10 μM), iron(10 μM) or PVD (10 μM) in M9 medium. When cells were treated with iron and PVD, the fluorescence of calcein-AM was quenched, indicating that the iron was transported inside the cell and the calcein-AM was able be quenched by iron inside this bacterium. While the bacteria were treated with a combination of bismuth, iron, and PVD, iron could not be rapidly transported within the cells, suggesting that bismuth might bind to PVD to inhibit iron transport. For Fig. a–i, the data are presented as mean ± SEM of three biological replicates. For Fig. g and i, P values were determined using two-sided unpaired t-test, 95% confidence interval.
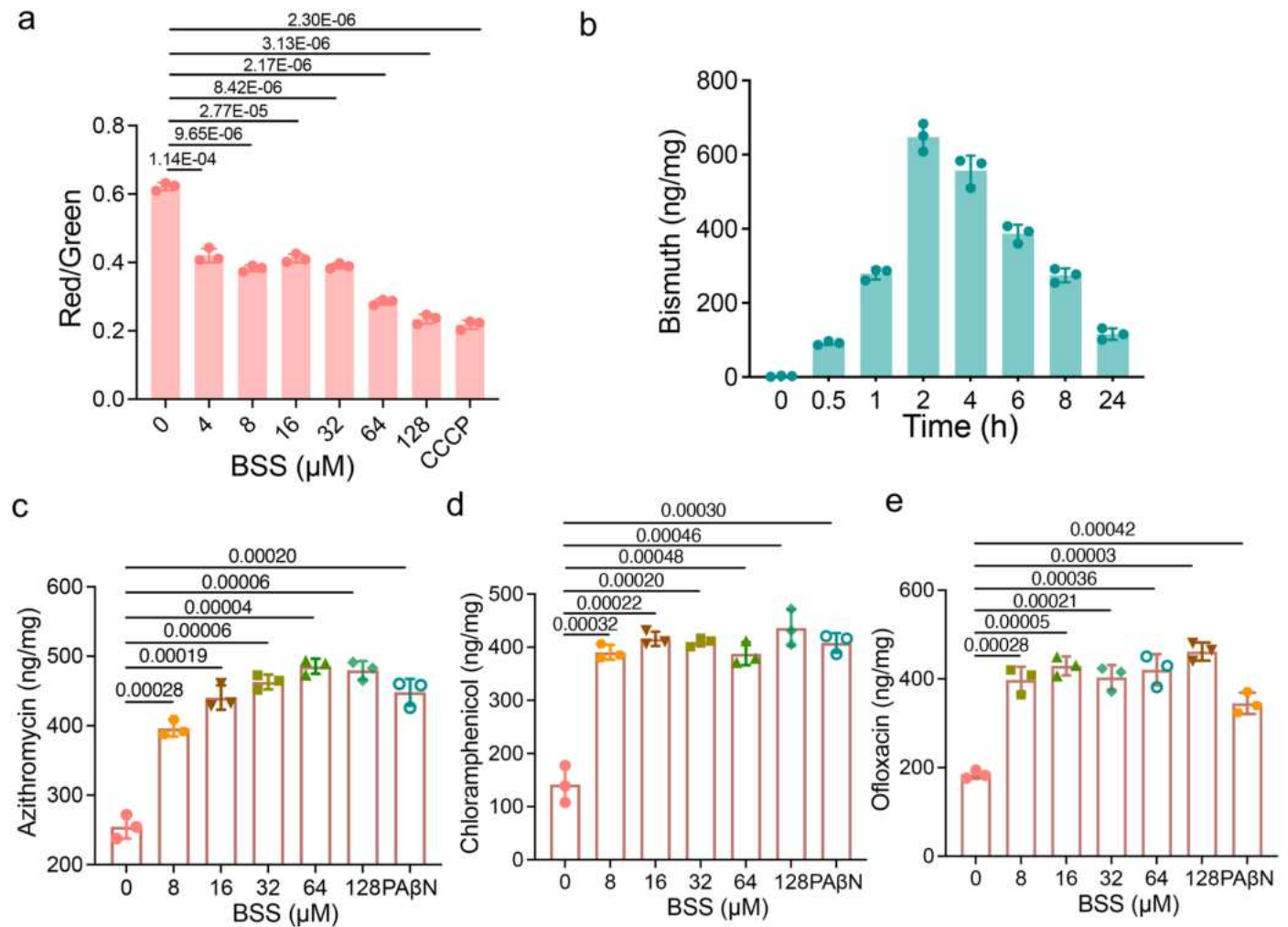
Extended Data Fig. 6 | Bismuth disrupts membrane potential and promotes intracellular antibiotic accumulation in *P. aeruginosa*. a, Detection of membrane potential in *P. aeruginosa*. Red/green ratios were calculated using population mean fluorescence intensities for *P. aeruginosa* incubated with 15 μM DIOC2(3) for 30 min in the presence of BSS or 20 μM CCCP. **b**, The time-based intracellular bismuth level of PAO1 under the treatment of 32 μM BSS. **c–e**, Intracellular BSS dose-dependent accumulation of azithromycin, chloramphenicol and ofloxacin. PAβN was used as a positive control. For Fig. a–e, the data are presented as mean ± SEM of three biological replicates. P values were determined using two-sided unpaired t-test for Fig. a, c–e.
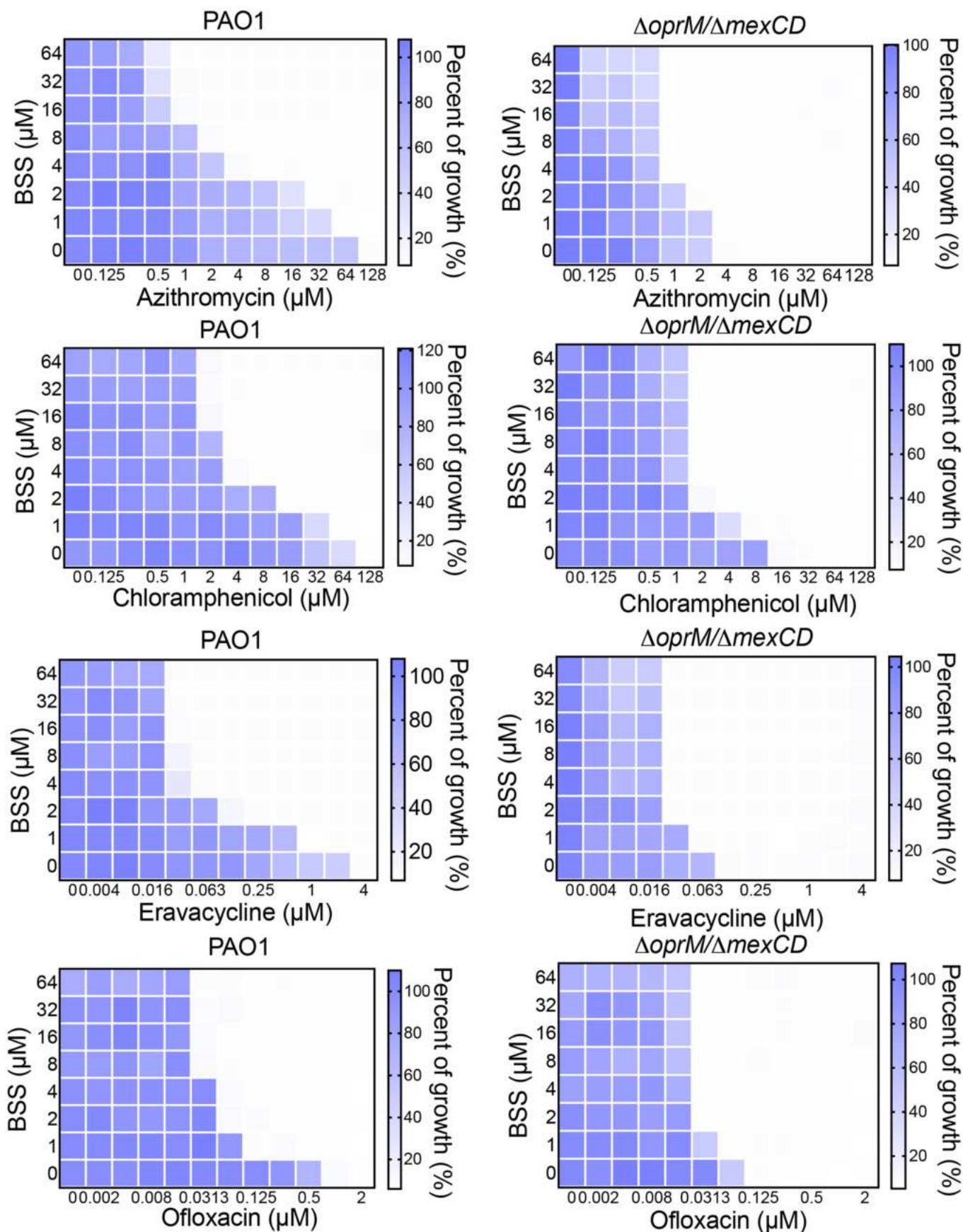
Extended Data Fig. 7 | The deletion of efflux pump genes *oprM* and *mexCD* antagonizes the synergistic effects of BSS and antibiotics. The heat map showing antagonized synergy of bismuth with eravacycline in the bacterial strain with efflux pump genes *oprM* and *mexCD* deleted.
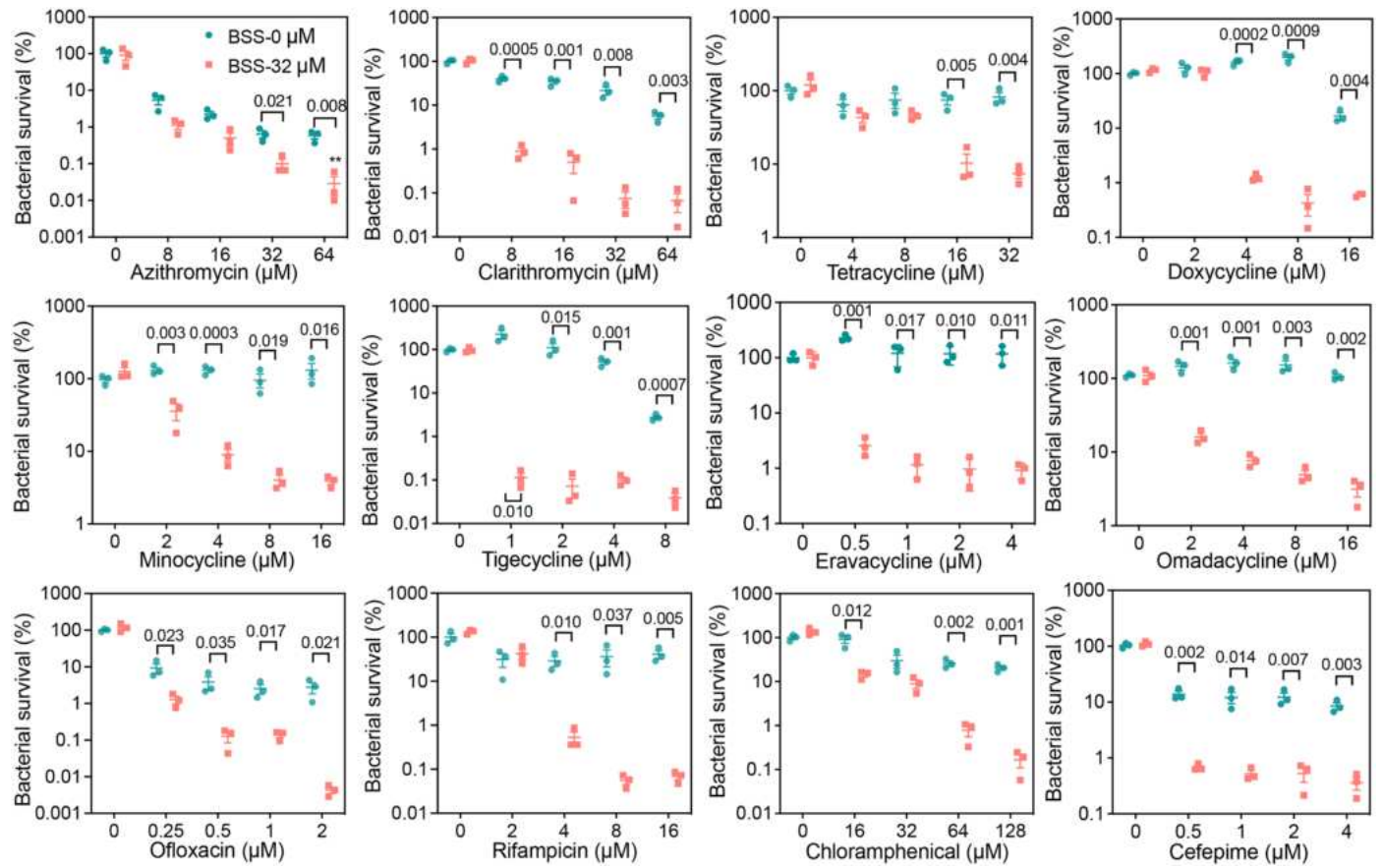
Extended Data Fig. 8 | Bismuth enhances the anti-biofilm abilities of antibiotics. The established biofilms were treated with antibiotics alone or combined with 32 μM of BSS for 24 hours. The biofilms were washed three times with sterile PBS and dispersed by ultrasound, the number of bacteria was determined by plating. The data are presented as mean ± SEM of three biological replicates. P values were determined using two-sided unpaired t-test.
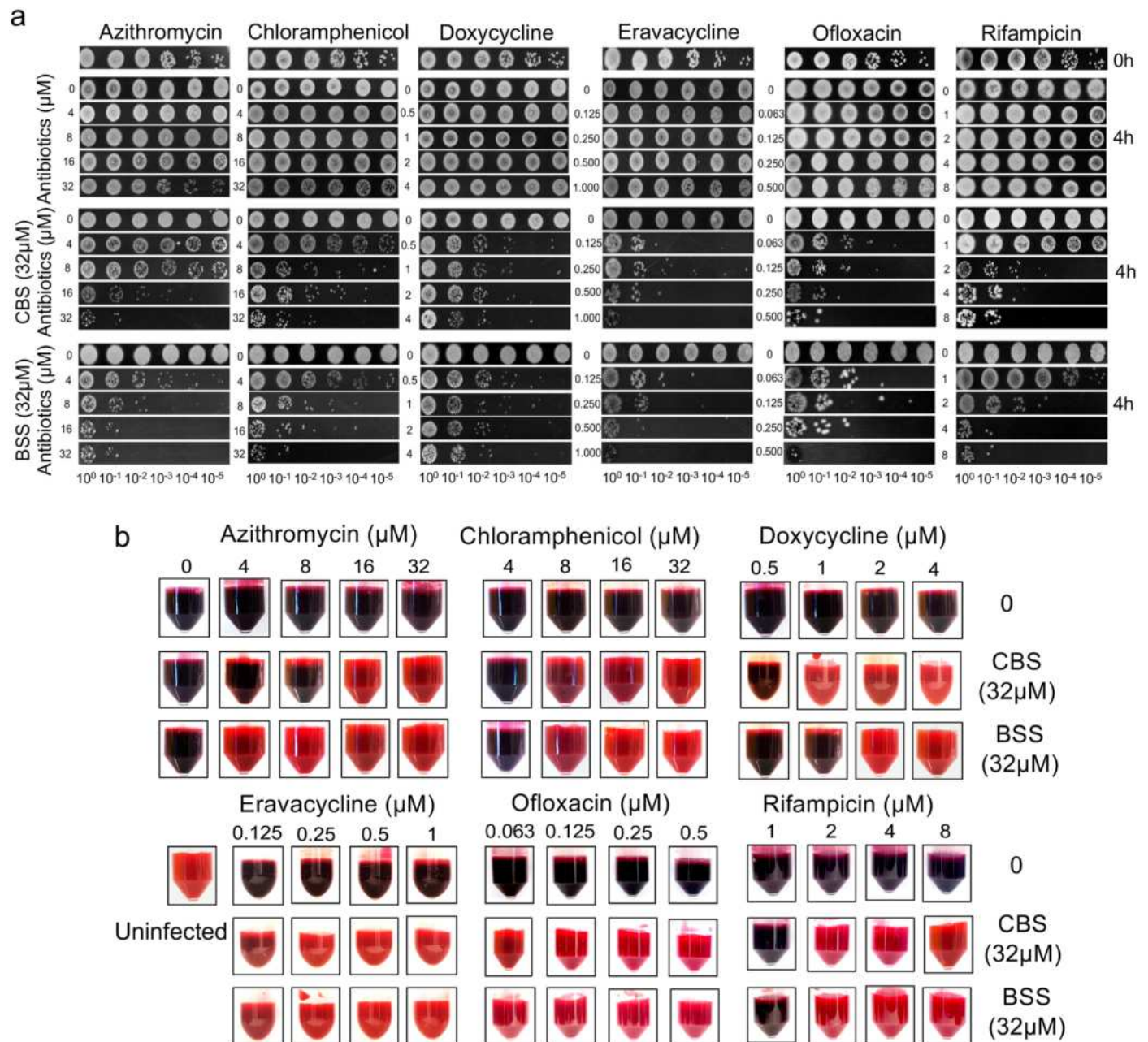
Extended Data Fig. 9 | Bismuth enhances the activities of antibiotics *ex vivo*. **a**, *Ex vivo* bacteremia model for antibiotics, bismuth drugs, and their combined antimicrobial activity. 10 µL of serial decimal dilutions of each one of the combinations of antibiotics with/without bismuth drugs (32 µM) tested in blood were dropped. All the tests were performed in triplicate. **b**, The appearance of the blood infected with PAO1 after treatment with the indicated concentration of antibiotics alone or the combinations with bismuth for 24 h. Black color of the blood indicates hemolysis and therefore bacterial growth. Red color of the blood indicates the therapy controlled the infection. All the tests were performed in triplicate.
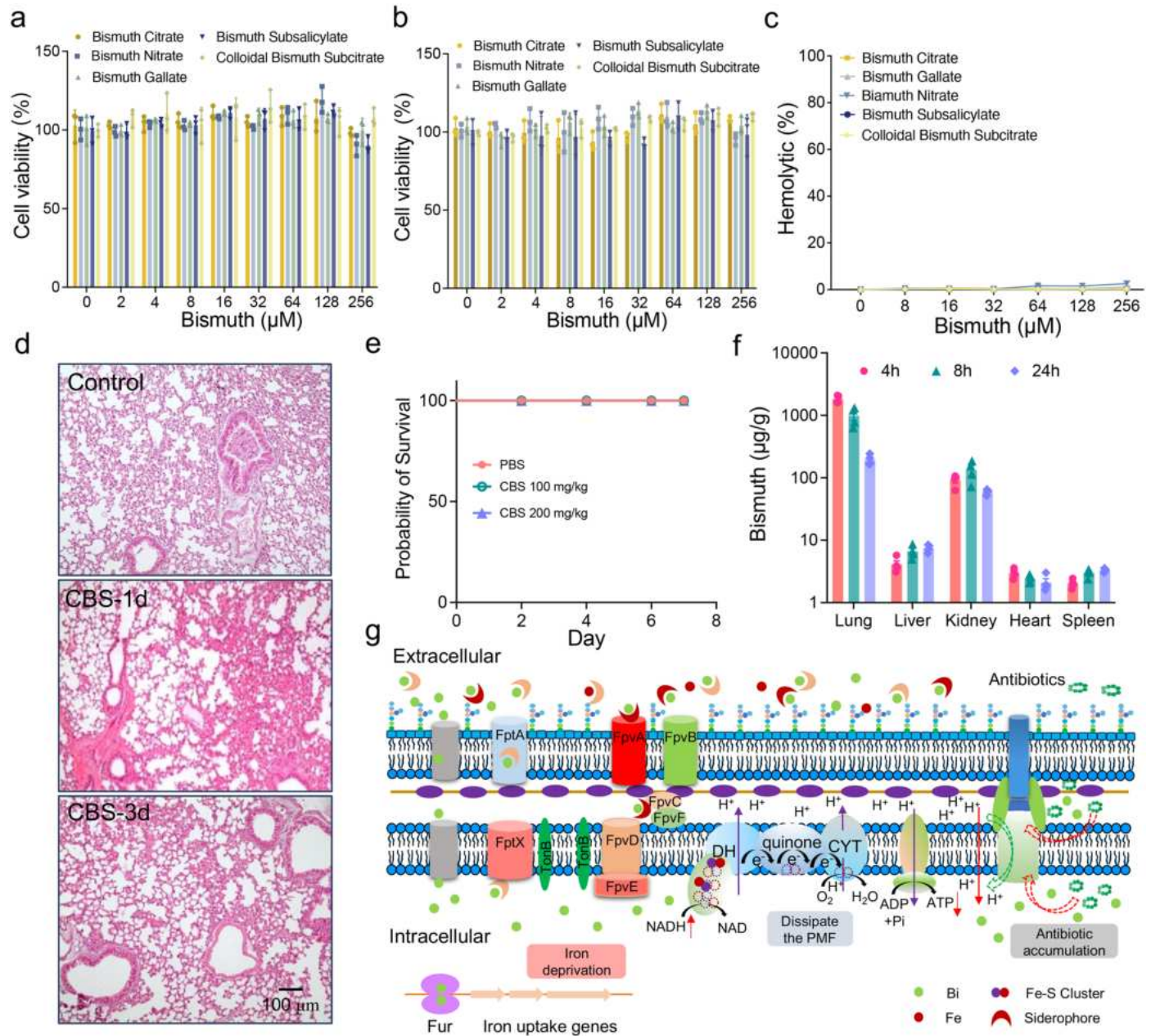
Extended Data Fig. 10 | Toxicity studies showing that bismuth drugs are not cytotoxic. a, **b**, Bismuth drugs show no toxicity in cells. The cell viability was measured by XTT assay under the treatment of different concentrations of bismuth drugs for 48 hours. The bismuth drugs showed negligible toxicity to human lung epithelial cells and embryonic kidney cells even at very high concentrations. **c**, Bismuth drugs show negligible hemolytic activity. Percent of hemolysis was calculated concerning the positive control (Triton X-100). (**a**–**c**) All the tests were performed in triplicate and all the data are presented as mean ± SD. **d**, Hematoxylin and eosin (H&E) staining of the mice lungs under treatment of single dose (-1d) or three doses (-3d) of 100 mg/kg CBS. **e**, Survival curves of mice treated with PBS, 100 mg/kg, and 200 mg/kg of CBS (n = 4) by the intranasal administration. **f**, The biodistribution of bismuth in mice after treatment by

the intranasal administration of 100 mg/kg CBS. **g**, Proposed the mechanism of action for the synergy of bismuth with antibiotics. Bismuth restores the susceptibility of *P. aeruginosa* to antibiotics through iron deprivation by interacting with siderophores and Fur. Consequently, the activity of iron-dependent cellular respiration complexes (for example, NADH dehydrogenase) is inhibited, resulting in dissipating the proton motive force (PMF), which further leads to repressed ATP synthesis and impaired multi-drug efflux pump. Ultimately, more antibiotics are rapidly accumulated inside bacterial cells, resulting in the death of cells. For Fig. a–c error bars represent mean ± SEM for three biological replicates. For Fig. d, four mice were included in each group, and similar results were obtained. For Fig. f error bars represent mean ± SEM for four mice samples.

Corresponding author(s): Hongzhe Sun

Last updated by author(s): Aug 1, 2024

Reporting Summary

Nature Portfolio wishes to improve the reproducibility of the work that we publish. This form provides structure for consistency and transparency in reporting. For further information on Nature Portfolio policies, see our Editorial Policies and the Editorial Policy Checklist.

Statistics

For all statistical analyses, confirm that the following items are present in the figure legend, table legend, main text, or Methods section.

n/a	Confirmed	
☐	☒	The exact sample size (n) for each experimental group/condition, given as a discrete number and unit of measurement
☐	☒	A statement on whether measurements were taken from distinct samples or whether the same sample was measured repeatedly
☐	☒	The statistical test(s) used AND whether they are one- or two-sided *Only common tests should be described solely by name; describe more complex techniques in the Methods section.*
☐	☒	A description of all covariates tested
☐	☒	A description of any assumptions or corrections, such as tests of normality and adjustment for multiple comparisons
☐	☒	A full description of the statistical parameters including central tendency (e.g. means) or other basic estimates (e.g. regression coefficient) AND variation (e.g. standard deviation) or associated estimates of uncertainty (e.g. confidence intervals)
☐	☒	For null hypothesis testing, the test statistic (e.g. F, t, r) with confidence intervals, effect sizes, degrees of freedom and P value noted *Give P values as exact values whenever suitable.*
☒	☐	For Bayesian analysis, information on the choice of priors and Markov chain Monte Carlo settings
☒	☐	For hierarchical and complex designs, identification of the appropriate level for tests and full reporting of outcomes
☒	☐	Estimates of effect sizes (e.g. Cohen's d, Pearson's r), indicating how they were calculated

Our web collection on statistics for biologists contains articles on many of the points above.

Software and code

Policy information about availability of computer code

Data collection	ICP-MS was performed by Agilent 7500a, Agilent Technologies, CA, USA; UV-vis spectra were recorded on a Varian Cary 50 spectrophotometer; Varioskan Flash; Thermo Scientific,Molecular imager ChemiDoc XRS + ,Bio-Rad.
Data analysis	Prism 9.0 (GraphPad Software Inc.),FastQC v0.11.9(Babraham Bioinformatics, Cambridge),Bowtie2 v2.4.2, SAMtools 1.11

For manuscripts utilizing custom algorithms or software that are central to the research but not yet described in published literature, software must be made available to editors and reviewers. We strongly encourage code deposition in a community repository (e.g. GitHub). See the Nature Portfolio guidelines for submitting code & software for further information.

Data

Policy information about availability of data

All manuscripts must include a data availability statement. This statement should provide the following information, where applicable:
- Accession codes, unique identifiers, or web links for publicly available datasets
- A description of any restrictions on data availability
- For clinical datasets or third party data, please ensure that the statement adheres to our policy

Data supporting the findings of this work are available within the paper, Supplementary Information files and source data files .

Research involving human participants, their data, or biological material

Policy information about studies with [human participants or human data](#). See also policy information about [sex, gender (identity/presentation), and sexual orientation](#) and [race, ethnicity and racism](#).

Reporting on sex and gender	NA
Reporting on race, ethnicity, or other socially relevant groupings	NA
Population characteristics	NA
Recruitment	NA
Ethics oversight	NA

Note that full information on the approval of the study protocol must also be provided in the manuscript.

Field-specific reporting

Please select the one below that is the best fit for your research. If you are not sure, read the appropriate sections before making your selection.

☒ Life sciences ☐ Behavioural & social sciences ☐ Ecological, evolutionary & environmental sciences

For a reference copy of the document with all sections, see [nature.com/documents/nr-reporting-summary-flat.pdf](#)

Life sciences study design

All studies must disclose on these points even when the disclosure is negative.

Sample size	3 samples/condition. In previous articles we demonstrated that 3 samples per condition provides data with statistical rigor(DOI: 10.1038/s41467-023-40828-3, DOI: 10.1038/s41467-021-23659-y,DOI: 10.1073/pnas.2119417119,DOI: 10.1038/s41564-020-00802-x) For mice experiments, 8 samples, In previous articles we demonstrated that 8 samples per condition provides data with statistical rigor(DOI: 10.1038/s41467-023-40828-3)
Data exclusions	No data were excluded
Replication	All experiments were performed with 3 biological and 3 technical replicates. Independent repetition of all experiments produced similar results.
Randomization	All experimental groups were allocated randomly
Blinding	While blinding is not relevant, extensive statistics and validation experiments all but guarantee the robustness of the dataset. The ethical concerns surrounding the use of bacteria and mice in experiments are much lower than those of human subjects. This means that there may be less of a need to use a double-blind experiment to reduce potential biases.Depending on the specific experimental design, it may be difficult or impossible to blind both the researcher and the participants to the experimental condition when working with bacteria.

Reporting for specific materials, systems and methods

We require information from authors about some types of materials, experimental systems and methods used in many studies. Here, indicate whether each material, system or method listed is relevant to your study. If you are not sure if a list item applies to your research, read the appropriate section before selecting a response.

Materials & experimental systems

n/a	Involved in the study
☒ ☐	Antibodies
☐ ☒	Eukaryotic cell lines
☒ ☐	Palaeontology and archaeology
☐ ☒	Animals and other organisms
☒ ☐	Clinical data
☒ ☐	Dual use research of concern
☒ ☐	Plants

Methods

n/a	Involved in the study
☒ ☐	ChIP-seq
☐ ☒	Flow cytometry
☒ ☐	MRI-based neuroimaging

Eukaryotic cell lines

Policy information about [cell lines and Sex and Gender in Research](#)

Cell line source(s)	HEK-293-T Cells and A549 cells were purchased from Sigma-Aldrich
Authentication	HEK-293-T Cell line and A549 cell line were authenticated by STR-PCR
Mycoplasma contamination	All cell lines tested negative for mycoplasma contamination
Commonly misidentified lines (See [ICLAC](#) register)	No misidentified cell lines were used.

Animals and other research organisms

Policy information about [studies involving animals](#); [ARRIVE guidelines](#) recommended for reporting animal research, and [Sex and Gender in Research](#)

Laboratory animals	6-8 weeks-old, female BALB/c mice, 8-10 weeks old, male C57Bl/6 mice. Mice rooms have 12-h dark-light cycle, the room temperature is around 24'C, and the humidity is kept at 45-65%
Wild animals	No wild animals were used in the study
Reporting on sex	No sex-based analyses have been performed. Murine Acute Pneumonia Model of Pseudomonas aeruginosa lung infection was performed in female BALB/c mice based on the protocol.
Field-collected samples	No Field-collected samples were used in the study
Ethics oversight	All animal experiments were approved by and performed in accordance with the guidelines approved by Committee on the Use of Live Animals in Teaching and Research (CULATR), the University of Hong Kong and the "Guide for the Care and Use of Laboratory Animals" as promulgated by the National Institute of Health, ARRIVE guidelines, and the protocols approved by the Ethics Committee of Laboratory Animals of the University of Granada.

Note that full information on the approval of the study protocol must also be provided in the manuscript.

Plants

Seed stocks	NA
Novel plant genotypes	NA
Authentication	NA

Flow Cytometry

Plots

Confirm that:

☒ The axis labels state the marker and fluorochrome used (e.g. CD4-FITC).

☒ The axis scales are clearly visible. Include numbers along axes only for bottom left plot of group (a 'group' is an analysis of identical markers).

☒ All plots are contour plots with outliers or pseudocolor plots.

☒ A numerical value for number of cells or percentage (with statistics) is provided.

Methodology

Sample preparation	The bacteria were cultured at 37°C in LB medium to an OD600 of 1. The bacteria were diluted to 106 CFU/ml in PBS. To each 1.5 ml of the bacterial suspension, 20 mM DiOC2(3) was added to achieve a final concentration of 15 μM and incubated for 1 h at 37°C in dark, followed by flow cytometry analysis (Accuri C6; BD). The DiOC2(3) was excited at 484 nm, and the emissions at 530 nm (green fluorescence) and 610 nm (red fluorescence) were measured. All experiments were performed in triplicate.

Instrument	Accuri C6; BD

Software	FCS Express 7

Cell population abundance	300,000 cells were collected for analyzing form each sample.

Gating strategy	For analysis, all P. seruginosa were gated based on SSC-H vs SSC-A for singlets. A more detailed strategy is included in supplementary fig 8

☒ Tick this box to confirm that a figure exemplifying the gating strategy is provided in the Supplementary Information.